Transonic Flow Around Swept Wings:

Revisiting Von Kármán's Similarity Rule

by

Jeffrey J Kirkman

A Thesis Presented in Partial Fulfillment
of the Requirements for the Degree
Master of Science

Approved April 2016 by the
Graduate Supervisory Committee:

Timothy Takahashi, Chair
Valana Wells
Marcus Herrmann

ARIZONA STATE UNIVERSITY

May 2016

ABSTRACT

Modern aircraft are expected to fly faster and more efficiently than their predecessors. To improve aerodynamic efficiency, designers must carefully consider and handle shock wave formation. Presently, many designers utilize computationally heavy optimization methods to design wings. While these methods may work, they do not provide insight. This thesis aims to better understand fundamental methods that govern wing design. In order to further understand the flow in the transonic regime, this work revisits the Transonic Similarity Rule. This rule postulates an equivalent incompressible geometry to any high speed geometry in flight and postulates a “stretching” analogy. This thesis utilizes panel methods and Computational Fluid Dynamics (CFD) to show that the “stretching” analogy is incorrect, but instead the flow is transformed by a nonlinear “scaling” of the flow velocity. This work also presents data to show the discrepancies between many famous authors in deriving the accurate Critical Pressure Coefficient (Cp*) equation for both swept and unswept wing sections. The final work of the thesis aims to identify the correct predictive methods for the Critical Pressure Coefficient.

TABLE OF CONTENTS

Page

LIST OF TABLES

Table Page

LSIT OF FIGURES

Figure Page

Figure Page

Figure . Page

Figure Page

INTRODUCTION

In the modern era of aircraft travel, speed and efficiency are vital aspects to the overall design. Aircraft are expected to fly faster, further and cheaper than their predecessors. Oddly, many of the fundamental aerodynamic principles to achieving these goals have not been revisited since the 1940s. This paper builds upon previous work done investigating simple sweep theory. It explores further into transonic flow effects using modern Computational Fluid Dynamics (CFD) analysis.

Traditionally designed transonic wings meet drag divergence criteria through spanwise variation of camber, incidence, and thickness. The formation of shock waves on the wing can have a multitude of effects that impact the performance of the aircraft. Weak shocks forming near the leading edge of the airfoil, if handled carefully, can increase the leading edge suction of the airfoil at the Critical Mach Number. If utilized properly, a shock wave, typically undesired due to the potential shock induced flow separation, can actually decrease drag due to favorable compressibility effects on axial pressure[1]. If the designer does not handle the shock wave properly, a strong shock may form that will separate the flow behind the shock wave, a phenomena known as shock induced flow separation. Because shock induced flow separation dramatically increases overall drag, wing designers take great care to ensure the formation of shock waves are carefully handled.

One approach to delaying the onset of the shock formation is to incorporate leading edge sweep. Wing sweep was first postulated in 1935 by the German, Adolf Busemann[2]. Busemann argued leading edge sweep could be used as a design option to delay the onset compressibility effects on the wing[2]. R.T. Jones was the first to present wing sweep in the United States[3]. Jones also postulated the advantages to wing sweep on compressibility effects, but hand waved through his explanations of the proper transformations[3,4].

In the work presented at the 2014 AIAA AVIATION conference, Takahashi, Dulin & Kady found inconsistencies in Busemann's Simple Sweep Theory[5]. In a continuation of this work, presented in 2015 AIAA AVIATION conference, Takahashi & Kamat employed modern CFD to revisit the inconsistencies[6]. They found evidence that the published methods to predicting the

onset of shock waves were inadequate. The data provided from the CFD runs did not inspire confidence that the classical theoretical predictions were applicable to real world swept wings.

In this current work, research starts with the effects of Von Kármán's[7] Transonic Similarity Rule, as explained by Schlichting[8], compares diverse author's research into the Critical Pressure Coefficient and Critical Mach number, and verifies the accurate sweep correction to the Mach dependent pressure coefficient. The end goal of this research is to determine the correct explanation and corrections for the flow characteristics around swept wings in transonic flight regimes.

The Transonic Similarity Rule holds that, for sub-critical flows, high speed flow around any arbitrary body may be represented by the incompressible, low speed flow, around a body with transformed geometry[8]. Over the years, many authors[3,4,7,8,9,10,11,12] have described this effect in terms of a geometrical "stretching" phenomenon. In this work, it became clear that the phenomenon exists, but that common explanations are logically inconsistent. This raises the question as to whether the mathematics of the Transonic Similarity Rule really means that a high speed aircraft is actually being "stretched" in the equivalent incompressible flow.

This paper documents evidence that shows that the Transonic Similarity Rule is a major oversimplification. Rather than stretching, there appears to be a Mach number dependent scaled velocity element.

In order to determine the correct formula for the Critical Pressure Coefficient, and therefore predict the Mach number associated with incipient supersonic flow, this work employed a variety of computational tools including commercial CFD (ANSYS Fluent)[13], 3D vortex lattice (VORLAX)[14], and popular 2D airfoil codes (JAVAFOIL)[15]. This paper will explore the fundamental works of Hermann Schlichting[8], Dietrich Küchemann[1], Eastman Jacobs[7] and Theodore Von Kármán[7] from a 2D perspective. The work done by modern authors[11,12,16,17] merely explain the research already performed and parrot the equations of these early authors. Although there are inconsistencies between the equations, there has not been much published work into further investigating on these estimations.

This work sets forth to determine the correct derivation for the Critical Pressure Coefficient. It finds that various published derivations lead to very different answers; although they all imply the same general physical trends. The inconsistencies between the various formulas at the Mach numbers in which real aircraft fly at, are significant enough to explain at least some of the problems noted by Takahashi & Kamat[6].

The final work done in this research overviews the sweep transformation for sheared wings. In the previous works of Takahashi, Dulin & Kady[5], and Takahashi & Kamat[6], there were inconsistencies from the simple sweep theory of Busemann[2]. Many authors such as Küchemann[1], Jones[3,4], Schlichting[8], and Neumark[18] have broadly agreed with Busemann[2] on his early findings, yet have found various equations and explanations for the critical conditions on swept wings. This thesis attempts to bring all the works of these famous authors together and determine which explanation is correct.

PRIOR ART

The early work of this thesis set forth the gather published work into transonic flows and their applicability to aircraft flight and performance.

Transonic Similarity Rules

In NACA Technical Memorandum 805, Prandtl addressed the flow of compressible fluids[9]. He postulates a geometric transformation to compare an incompressible flow, to a compressible flow[9]. Prandtl argued a Mach number dependent “stretching” on the components in transonic flow. This geometrical “stretching” has been used as the explanation for the increased effectiveness of aircraft components in the transonic regime. This work provides a conceptual path to design aircraft that operate in the transonic regime. It is also the basis of many general purpose potential flow aerodynamic flow solvers.

Prandtl’s key equation for transonic potential flow can be found in equation 10 in the original manuscript (reproduced here as equation 1):

$$\frac{\delta u}{\delta x}\left(1-\frac{{u_0}^2}{c^2}\right)+\frac{\delta v}{\delta y}+\frac{\delta w}{\delta z}=0 \quad (1)$$

In this equation, *u*, *v*, and *w* refer to components of velocity in the *x*, *y*, and *z* directions respectively. This becomes the basis of modified potential flow equations. The u_0 refers to the freestream flow velocity in the *x* direction and *c* is the speed of sound of the flow. This equation provides a freestream velocity dependent (Mach number) correction on the flow in the *x*-direction.

This is a powerful equation. The only assumptions are that the velocities derived are small compared to the flow, u_0, and that the velocity in the *v* and *w* direction are small relative to the speed of sound, *c*. This thesis does not dispute the utility of this equation, merely challenges the popular physical explanations of its action.

Four possible physical explanations can arise from this equation (see Figure 1). All invoke the famous, Prandtl-Glauert (P-G) scaling parameter: (equation 2)

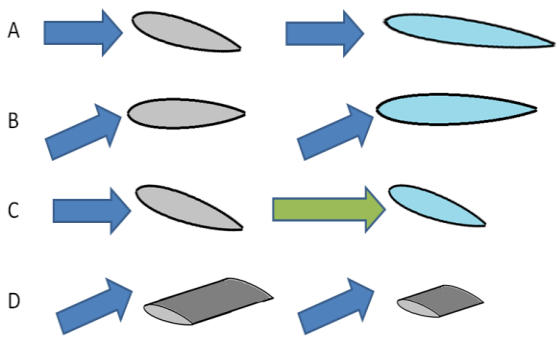

Figure 1. Possible geometry implications of the Prandtl-Glauert potential flow equation.

$$\beta=\sqrt{1-\frac{u_0^2}{c^2}}=\sqrt{1-{M_\infty}^2} \quad (2)$$

One interpretation (represented by Figure 1A) says that the scaling term acts upon the *x* axis dimension of the geometry terms, in other words, P-G scales the longitudinal geometry in the axis of on-coming flow by a factor proportional to the reciprocal of β, $1/\sqrt{1-M_\infty^2}$. Here, the inflow velocity is exactly aligned with the *x* axis; thus a wing at angle-of-incidence must be represented by an inclined geometry. Therefore, the *x* axis stretching results in the equivalent incompressible shape being longer in the *x*, or chordwise direction but no longer in the *y*, or thickness direction. Such a transformation implies that the equivalent incompressible shape has greater effective

area, a lower effective thickness-to-chord ratio (*t/c*), and a lower incidence (α) than the actual high-speed shape.

A second possible interpretation (represented by Figure 1B) says that the scaling term acts upon the *x* axis dimension of the geometry terms. In other words, P-G scales the longitudinal geometry in the axis of on-coming flow by a factor proportional to the reciprocal of β, $1/\sqrt{1-M_\infty^2}$. In this view, the geometry is exactly aligned with the *x* axis; but the inflow velocities comprise a steady flow in both the *x* and *y* directions; *u* and *v* are non-zero. Thus, the *x* axis stretching results in the equivalent incompressible shape being longer in the *x*, or chordwise direction but no longer in the *y*, or thickness direction. Such a transformation implies that the equivalent incompressible shape has greater effective area, a lower effective thickness-to-chord ratio (*t/c*), and the same incidence (α) than the actual high-speed shape.

The third interpretation (represented by Figure 1C) says that the scaling term acts upon the *u* dimension of the flow terms, in other words, P-G scales the effective flow speed by a factor proportional to β, simply $\sqrt{1-M_\infty^2}$. In this view, the inflow perfectly aligns itself with the *x* axis. The geometry is inclined to represent incidence; however, no Mach number dependent "stretching" takes place. A velocity scaling viewpoint has the equivalent incompressible shape maintain the same area, incidence and thickness-to-chord ratio as the actual high-speed shape. However, the scaled effective velocity means that the actual pressure coefficients (along with lifting forces, pressure drag forces and pitching moments) increase in a manner proportional to $1/\sqrt{1-M_\infty^2}$.

The final interpretation (represented by Figure 1D) says that the scaling term acts upon the *y* axis dimension of the geometry terms, in other words, P-G scales the transverse geometry in the axis of on-coming flow by a factor proportional to β, $\sqrt{1-M_\infty^2}$. Thus, the *y* axis stretching results in the equivalent incompressible shape being shorter in the *y*, or spanwise direction but no longer in the *x*, chordwise or, *z*, thickness direction. Such a transformation implies that the equivalent incompressible shape has the same incidence and thickness-to-chord ratio (*t/c*) as the actual high-speed shape, but a smaller area and lower aspect ratio.

Prandtl[9] solves the modified form of this equation, an elliptic equation for subsonic velocities and hyperbolic for supersonic velocities, to explain the geometric transformation implied by high-speed, compressible (but subcritical) flows. Prandtl states that in order for a contour in a compressible fluid to maintain the same result as in an incompressible fluid, the "contour must be made thinner"[9] and likewise, the angle of attack must decrease. This is, in essence interpretation 1A as stated above.

It is interesting to note that Prandtl describes this work as being a geometrical change. He of course talks about comparing a compressible solution back to an incompressible one, where as other authors (Göthert[10], Schlichting[8], and Drela[12]) view it in reverse; taking an incompressible solution and correcting to a compressible one. Prandtl's primary discussion is how it relates to a contour thickness as well as an angle of attack change. It appears to be an attempt to make sense of the work he laid out with only a slight comment on the correction factor being related to the velocities themselves. Prandtl "hand waves" the discussion to relate a mathematical model to some form of a physical relationship.

Although less famous than Prandtl, Göthert made considerable contributions to the theory of three-dimensional flows at high subsonic speeds. In NACA TM-1105 from 1946[10], Göthert discussed the effects of apparent geometric "stretching" and incompressible solution in order to obtain the compressible flow solution. Reproduced as equation 3 is Göthert's version of the potential flow equation:

$$\frac{\partial^2 \phi_c}{\partial x_c^2} + \frac{\partial^2 \phi_c}{(\sqrt{1-\mathrm{M}\infty^2} \times \partial y_c)^2} + \frac{\partial^2 \phi_c}{(\sqrt{1-\mathrm{M}\infty^2} \times \partial z_c)^2} = 0 \qquad (3)$$

Göthert claims that the streamlines of a compressible flow are distortions of the streamlines of the incompressible by a "Prandtl Factor" of $1/\sqrt{1-M_\infty^2}$, but in the *y* and *z* directions (as opposed to a reciprocal transformation in the *x* direction). Göthert argues that the compressible flow is comparable to the incompressible flow by a decrease in the *y* and *z* contours. Therefore, his "stretching" of the incompressible profile is actually a contraction along the *y* and *z* coordinates (the *x* coordinate is defined in the free stream direction).

R.T Jones first approached Prandtl's transformation in NACA TR-863[3]. He refined these ideas in High Speed Wing Theory[4] co-authored by Cohen. He explains transonic similarity as a transformation in two dimensions as a stretching in the *x*-direction by the factor of $1/\sqrt{1-M_\infty^2}$. Therefore, it is the chord of the airfoil that the Mach number dependent stretching is applied to. This explanation is purely geometrical and only occurs in the *x*-direction. Jones & Cohen go on to argue the transformation is applicable to a three-dimensional wing as well[4].

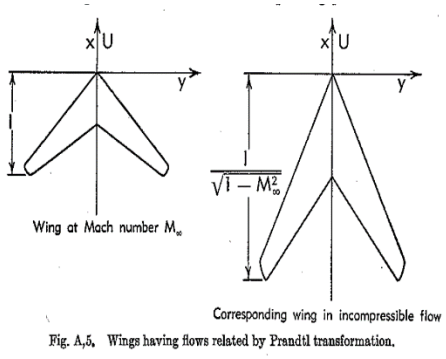

Fig. A,5. Wings having flows related by Prandtl transformation.

Figure 2. Jones & Cohen explanation of the Prandtl-Glauert stretching. Reproduced from Jones, R. T., & Cohen, D. (1960). *High speed wing theory*. Princeton, NJ: Princeton University Press.

According to Jones & Cohen[4], the compressible flow relationships that govern a two-dimensional wing sections apply broadly to three-dimensional wings (see Figure 2). They state that, geometrically, the longitudinal stretching means that the equivalent area increases while the span remains the same. Thus both the effective sweep angle and the aspect ratio of the equivalent incompressible wing will vary due to the "stretching" in the chord. They hold that the aspect ratio of a compressible wing is comparable to a smaller aspect ratio wing in incompressible flow. Thus the effective incompressible area increases by the Prandtl-Glauert factor, $1/\sqrt{1-M_\infty^2}$, while the effective incompressible aspect ratio declines by a factor of $\sqrt{1-M_\infty^2}$. Jones does not expressly differentiate between Figure 1A and Figure 1B physical analogies in either work [3,4]. Because he does not discuss angle-of-attack effects directly, either explanation could fit his reasoning.

Hermann Schlichting also approaches the "stretching" transformation as a similarity rule[8]. Schlichting holds that the following geometrical transformations apply to compare a wing in

compressible flow to an equivalent wing in incompressible flow. First, he applies a “stretching” on the spanwise, *y*, direction:

$$x_{inc} = x \tag{4a}$$

$$y_{inc} = y \cdot \sqrt{1 - M_\infty{}^2} \tag{4b}$$

$$z_{inc} = z \tag{4c}$$

Thus, he implies the following properties of a transformed wing: that the span, *b*, scales with increasing Mach number but the chord remains constant.

$$b_{inc} = b \cdot \sqrt{1 - M_\infty{}^2} \tag{5a}$$

$$c_{inc} = c \tag{5b}$$

This means that the aspect ratio, AR, declines with increasing Mach number, while the taper ratio, TR, thickness-to-chord ratio, t/c, and effective angle of attack, α, all remain constant:

$$AR_{inc} = AR \cdot \sqrt{1 - M_\infty{}^2} \tag{6}$$

$$TR_{inc} = TR \tag{7}$$

$$\left(\frac{t}{c}\right)_{inc} = \left(\frac{t}{c}\right) \tag{8}$$

$$\alpha_{inc} = \alpha \tag{9}$$

Unlike Prandtl[1], Schlichting transforms the wing at compressible flow speeds into an equivalent incompressible wing by transforming the *y* coordinate; he does not discuss the *z* coordinate in his transformations. Mathematically it is algebraic rearrangement of terms first shown by Prandtl[1] that follows the method proposed by Göthert[2]. Although the explanation differs from Prandtl, the physical implications remain the same.

Similar to Jones & Cohen[4], Schlichting[5] indicates that the effective sweep of the incompressible wing increases with increasing Mach number although for different reasons (stretching in the spanwise as opposed to chordwise direction):

$$\cot(\varphi_{inc}) = \cot(\varphi) \cdot \sqrt{1 - M_\infty{}^2} \tag{10}$$

The effects of these transformations may be seen in Figures 3, 4 and 5. These figures show the Mach depended transformations on the Aspect Ratio and sweep as postulated by Jones & Cohen[4] and independently by Schlichting[8].

Figure 3 plots equation 6 and finds, at higher Mach numbers, that the equivalent incompressible wing has a lower Aspect Ratio than the physical wing. Therefore as the Mach number increases the wing in the compressible flow acts as a incompressible wing with a larger Aspect Ratio.

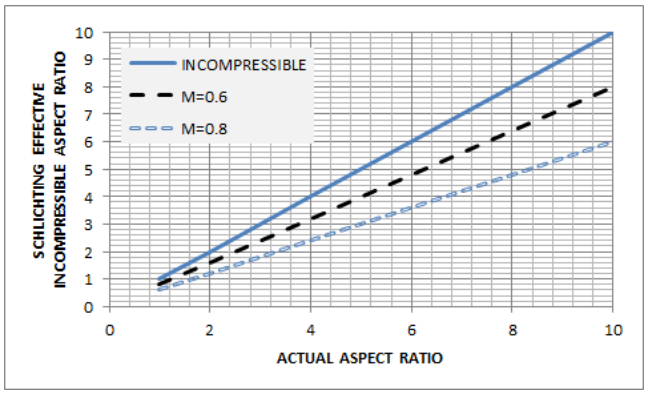

Figure 3. Schlichting / Jones & Cohen explanation of the Prandtl-Glauert stretching effects on Aspect Ratio.

Figure 4 demonstrates how equation 10 affects the effective sweep. As the Mach number increases, Schlichting's rule finds that swept wings behave as if they were incompressible wings of greater sweep (and smaller span). Therefore, as the Mach number increases the equivalent sweep of the wing increases as well.

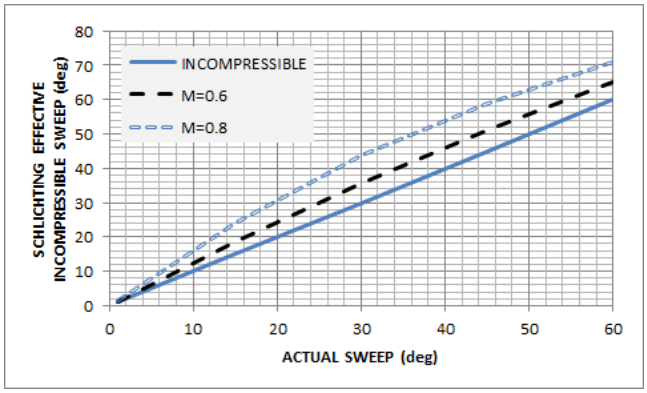

Figure 4. Schlichting / Jones & Cohen explanation of the Prandtl-Glauert stretching effects on sweep.

Figure 5 shows the geometric transformations described by Schlichting[8]. This figure may be interpreted to illustrate how a "given" physical wing can be represented by a series of "transformed" or equivalent incompressible wings. Because Schlichting holds that $y_{inc} = y * \sqrt{1 - M_{\infty}^2}$, his equivalent incompressible wing is of a smaller wingspan (and area) than that of the physical wing in compressible flow. This is a key point where Jones and Schlichting differ. Jones[3,4] implies that an increase in Mach number leads to an equivalent incompressible wing of greater effective area. Schlichting[8] states that an increase in Mach number leads to an equivalent incompressible wing of lesser effective area. Clearly, both analogies cannot be correct!

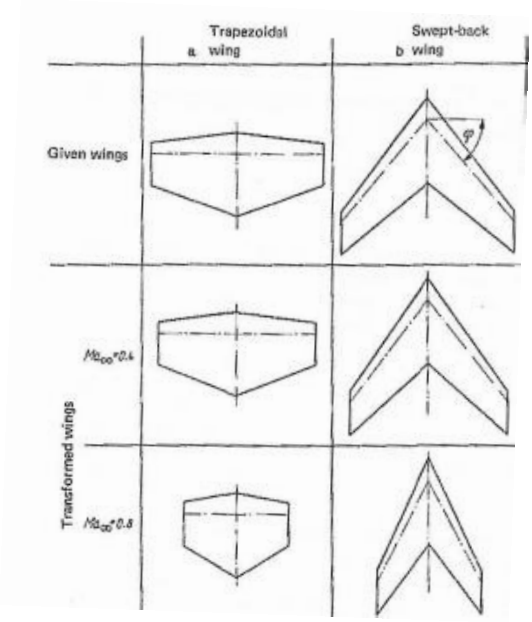

Figure 5. Schlichting's graphical explanation of the Transonic Similarity Rule. Adapted from Schlichting, H., & Truckenbrodt, E. (1979). *Aerodynamics of the Airplane* (H. J. Ramm, Trans.). McGraw-Hill. Pg. 266

Thus, Schlichting's argument indicates that he basically follows the guidelines of Figure 1D; changes in Mach number impact the effective span and area of the wing, but not the incidence or thickness.

In other areas, Schlichting's[8] transformations agree with the work of Jones & Cohen[3,4]. They both argue an equivalent incompressible wing has a lower aspect ratio compared to the

compressible wing. The difference occurs is how the incompressible solution is “stretched”. Schlichting states that the stretching occurs along the *y*-axis, therefore changing the aspect ratio, the span, and even changing an equivalent sweep angle.

One major point that Schlichting makes is: for the unchanged profile (airfoil) between incompressible and compressible flow, the angle of attack will be the same. This is an interesting point that Schlichting makes. Many of these ideas are similar to Jones. Although Jones does not talk specifically about the angle of attack transformations, he agrees with Schlichting on the changes in sweep and Aspect Ratio.

Schlichting[8] continues in his derivations of the transformation of the lift coefficient, pressure coefficient, and moment coefficient of the incompressible wing to those of the compressible wing. He does not give an explanation as to the reason for this, but he also does not consider a *z*-direction transformation in any of his work. Schlichting only concerns himself with the *x*-*y* plane in his transformations. This is similar to the work of Prandtl[9], Göthert[10], and Jones[3,4]. Prandtl only considers the transformation in the *x*-axis with an assumption that the velocities in the *y* and *z* axes are small relative to the speed of sound. Göthert reverses this explanation slightly and argues that the transformation occurs on the *y* and *z* axis. Either way the early works into transonic flow transformations made simplifying assumptions to remain in a two dimensional plane.

Schlichting also holds the following transformation formulas to hold for an “inclined wing of finite span in subsonic flow” where $\alpha = \alpha_{inc}$ where the geometry at incompressible speeds is otherwise identical to that at compressible speeds:

$$Cp = \frac{1}{\sqrt{1-{M_\infty}^2}} \cdot Cp_{inc} \tag{11}$$

$$CL = \frac{1}{\sqrt{1-{M_\infty}^2}} \cdot CL_{inc} \tag{12}$$

$$\frac{dCL}{d\alpha} = \frac{1}{\sqrt{1-{M_\infty}^2}} \cdot \left(\frac{dCL}{d\alpha}\right)_{inc} \tag{13}$$

$$\alpha_0 = \alpha_{0_{inc}} \tag{14}$$

$$Cm = \frac{1}{\sqrt{1-{M_\infty}^2}} \cdot Cm_{inc} \tag{15}$$

$$CD_i = \frac{1}{\sqrt{1-{M_\infty}^2}} \cdot {CD_i}_{inc} \tag{16}$$

That is, the pressure coefficients at high speeds increase inversely proportional to the Prandtl-Glauert scaling parameter, β; the lift coefficient at any given angle-of-attack increase inversely proportional to β; the slope of the lift coefficient with respect to angle-of-attack increases inversely proportional to β; the zero-lift-angle of attack remains unchanged, and the induced drag coefficient increases inversely proportional to β. It therefore follows that the inviscid aerodynamic efficiency at a given angle of attack, C_L/C_{Di} should not change as a function of *Mach* number because both the lift and induced drag coefficient scale directly with the reciprocal of β. Schlichting's arguments are inconsistent with those shown earlier in his book; they more closely follow the transformation implied by Figure 1C.

The works of Prandtl[9], Göthert[10], Jones[3,4] and Schlichting[8] have been revisited more recently. Various authors, such as McLean[11] and Drela[12], agree that a Mach number dependent "stretching" transformation occurs, yet they disagree on which explanation is correct.

The explanation given by Doug McLean in his book Understanding Aerodynamics[11] very briefly covers "stretching" as Jones and Prandtl would call it. McLean states that the pressure disturbances produced by an airfoil will maintain the general characteristics, however they will gradually increase. He does not call this a "stretching", but instead just points out the increase in the pressure distribution in a compressible flow, compared to an incompressible flow.

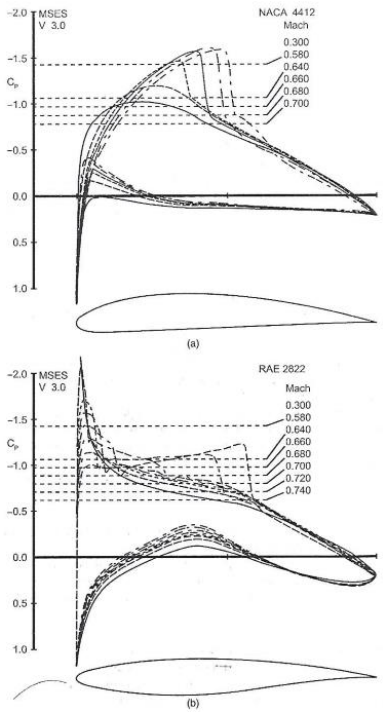

Figure 6. McLean's description of relationship between shock wave formation and *Cp**. Reproduced from McLean, D. (2013). 7.4.8 Airfoils in Transonic Flow. In *Understanding Aerodynamics* (pp. 342-350). John Wiles & Sons.

Thus, McLean[11] circumstantially implied that flow behaves along the lines of Figure 1C. Figure 6 from Mclean[11], shows the effect of the Mach number on the pressure distributions. The airfoil remains at a constant angle of attack; however, the pressure distributions appear as though the airfoil is "thicker" as the Mach number increases. This is the perfect example to McLean's discussion on the change in the pressure coefficient in compressible flow. These arguments also seem to imply the existence of an effective dynamic pressure transformation, more than any formal geometric morphing.

Mark Drela's[12] work in Flight Vehicle Aerodynamics explains the Prandtl-Glauert Transformation in a modified form. Drela defines the scaling factor as $\beta = \sqrt{1 - M_\infty^2}$ and uses this β to define the geometrical transformations, but instead of Prandtl's transformation in the *x*-direction, or Schlichting's transformation in the spanwise, *y*, direction, he applies transformations in both the *y* and *z*-directions.

Drela[12] applies these transformations to the *y* and z-directions, because he transforms the compressible flow back to the incompressible solution. Therefore, he argues that the *y* and *z* coordinates decrease in the incompressible flow, when compared to the compressible flow solution. The incompressible angle of attack is decreased as well as the aspect ratio. In the figure below, Drela shows the real flow transformed into a mathematically equivalent flow

Drela[12] sketches the geometric transformations in his writings, reproduced here in Figure 7. Drela shows that the real flow (compressible) can be transformed to an incompressible flow through a decrease in the angle of attack, a decrease in the *z*-direction (including airfoil thickness), and the *x*-direction remaining untouched.

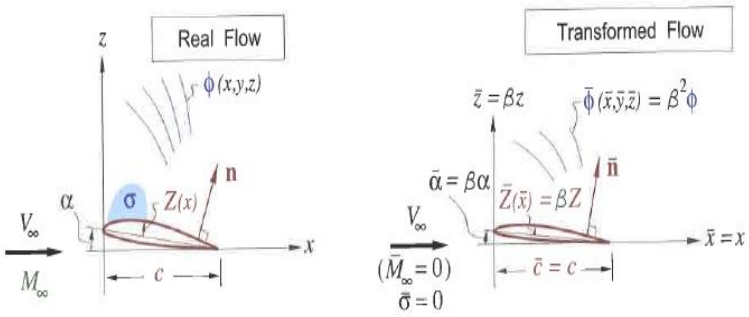

Figure 7. Drela's sketch of the transformed equivalent incompressible geometry showing an increase in area and decrease in angle-of-attack. Reproduced from: Drela, M. (2014). 8.6 Prandtl-Glauert Analysis. In *Flight Vehicle Aerodynamics* (pp. 173-180). MIT Press.

Each author above has a different explanation on the stretching and how it applies to the equivalent incompressible geometry. Although many of the transformations are mathematically equivalent, there is a disconnect between the explanations of this "stretching". Jones and Schlichting appear to agree with one another on many of the "stretching" transformations in the end, however their axes differ slightly. In terms of the sweep and Aspect Ratio the two authors agreed upon the final result, yet Schlichting argues a stretching on the span and Jones argues a stretching on the chord. Although the final result is the same, these two cannot both be right! Prandtl and Göthert fundamentally agree in the stretching, yet provide explanations for stretch on different axes! Göthert's[10] transformations, backed by Drela[12], are applied to the *y* and *z* axis where Prandtl[9] only applies the transformation on the *x* axis. McLean[11] disagrees with everyone's

explanation of a geometrical transformation and argues that the differences in the flow is due to a dynamic pressure “stretching”.

Even when the authors cite another as the source of their “stretching”, they come out as different interpretations! This starts to make one wonder, who is right on the transformation and what is the correct physical explanation?

This thesis will validate many of these relationships using modern computational methods.

Critical Pressure Coefficient

To properly design transonic wings, engineers must pay careful consideration to match the flight conditions where incipient shock wave occurs with the planned operating characteristics of the airplane. This is due to the large drag impact that a shock wave can produce when it induces flow separation.

The point where a shock wave begins to form is the Critical Mach Number of the wing, the Mach number in which sonic flow is first attained somewhere on the wing.

Traditionally, this phenomenon is associated with the speed where the peak underpressure of the local airflow falls below the Critical Pressure Coefficient (*Cp**). It is critical to precisely capture the speed and lift coefficient where this occurs because the overall design of a wing hangs in the balance of being able to properly meet design performance targets in terms of lift and drags well as the necessary volume for structure, fuel and other components.

Theodore Von Kármán, in his famous paper on compressibility effects[7], uses Glauert’s approximation[19] to derive his equation for the Critical Pressure Coefficient. Glauert’s approximation allows the mathematician to linearize the perturbation velocities under an argument that holds that while higher order perturbation terms exist, they are negligible. This leads Von Kármán, to derive his equation for the Critical Pressure Coefficient:

$$Cp^* = \frac{2\left[\left(1-M_\infty^2\right)^{3/2}\cdot\left(1+M_\infty^2\right)^{1/2}\right]}{M_\infty} \tag{17}$$

Kármán goes on to state that the equation above may not be exact due to the derivation from the linear theory.

Kármán[7] suggests that Eastman Jacobs' derivation from the thermodynamic relationship is a good starting point for an improved prediction method.

$$Cp^* = \frac{2\left[1-\left(\frac{2+(\gamma-1)M_\infty^2}{\gamma+1}\right)^{\gamma/(\gamma-1)}\right]}{\gamma M_\infty^2} \tag{18}$$

Kármán points out that Jacobs included some necessary corrections to errors introduced by the linearized theory. Interestingly, a direct source has not been found of this derivation on scholar.google.com. None of Eastman Jacobs' authored papers seem to explain his rationale.

Interestingly, while Jacobs worked for the NACA, the Critical Mach Number lines in the famous NACA TR-824[20] airfoil guide follow Von Kármán's equation (equation 17) to infer the Critical Mach Number from the peak recorded underpressure found during low speed testing.

John Anderson, in Introduction to Flight, approached the Critical Pressure Coefficient using thermodynamic relationships[16]. Anderson derives equation 19 as an estimate of the pressure coefficient and the isentropic relationships between the static pressure and total pressure.

$$Cp^* = -\frac{2}{\gamma M_\infty^2}\left\{\left[\frac{2+(\gamma-1)M_\infty^2}{\gamma+1}\right]^{\gamma/(\gamma-1)} - 1\right\} \tag{19}$$

This relationship is valid for any flow for a given freestream Mach number. As the Freestream Mach number approaches 1, the critical pressure coefficient in this equation approaches 0, as expected.

Schlichting's[8] definition of the Critical Pressure Coefficient relies on the knowledge of the Critical Mach Number. Schlichting argues that if the Critical Mach Number is known, then the Critical Pressure Coefficient can be easily determined by the minimum pressure coefficient on the surface. He does make a correction to his equation as well into include the sweepback of the wing. Reproduced below is Schlichting's derivation for the Critical Pressure Coefficient on the wing:

$$Cp^* = -\frac{2}{\gamma+1}\frac{1-Ma_{\infty_{cr}}^2(\cos\varphi)^2}{Ma_{\infty_{cr}}^2} \tag{20a}$$

For simple two-dimensional flow, Schlichting's equation reduces to:

$$Cp^* = -\frac{2}{\gamma+1}\frac{1-Ma_{\infty_{cr}}^2}{Ma_{\infty_{cr}}^2} \tag{20b}$$

This is a notably simpler equation than proposed by either von Kármán or Jacobs.

Küchemann[1] in his famous book, The Aerodynamic Design of Aircraft, describes the critical conditions through the use of isobars on a swept wing. He argues that on a swept wing the critical condition occurs where the flow normal to the isobars reaches the local speed of sound. Küchemann uses his swept wing example to derive through the thermodynamic relationships between pressure, velocity, and total head to reach the equation below.

$$Cp^* = \frac{2}{\gamma M_\infty^2}\left\{\left(\frac{2}{\gamma+1}\right)^{\frac{\gamma}{\gamma-1}}\left(1+\frac{\gamma-1}{2}M_\infty^2\,(\cos\varphi)^2\right)^{\frac{\gamma}{\gamma-1}}-1\right\} \tag{21a}$$

Which, when simplified for simple two-dimensional flow, reduces to:

$$Cp^* = \frac{2}{\gamma M_\infty^2}\left\{\left(\frac{2}{\gamma+1}\right)^{\frac{\gamma}{\gamma-1}}\left(1+\frac{\gamma-1}{2}M_\infty^2\right)^{\frac{\gamma}{\gamma-1}}-1\right\} \tag{21b}$$

Although argued from a different perspective, and algebraically distinctive, Küchemann's equation (21b) turns out to be numerically identical to the Eastman Jacobs equation (18) cited by Kármán[7].

An accurate estimate of the Critical Pressure Coefficient is crucial to predict incipient shock wave formation on a transonic wing. Although many prior authors above apply similar, if not identical basic governing physics, each author follows a personal path to arrive at fundamentally different final equations which supposedly estimate *Cp**.

The inconsistencies between each derivation inspires no hope in the design process to accurately predict the shock wave formation.

These famous equations (Schlichting (20b), von Kármán (17), Küchemann (21b), E. Jacobs (18) and Anderson (19)) are plotted together as Figure 8. Although the equations vary, they each maintain the basic physical constraints. For example, each equation approaches zero as the Mach number approaches one. Therefore, as the freestream flow approaches sonic

velocity, the pressure coefficient relating to the sonic flow point is zero. When the free stream flow is at Mach 1, any disturbance that leads to increased velocities and reduced pressures triggers a shock wave. It is also interesting to note that for two dimensional flow, Küchemann, Eastman Jacobs, and Anderson's Critical Pressure Coefficients are mathematically equivalent. This is expected since they are all derived through thermodynamic relationships.

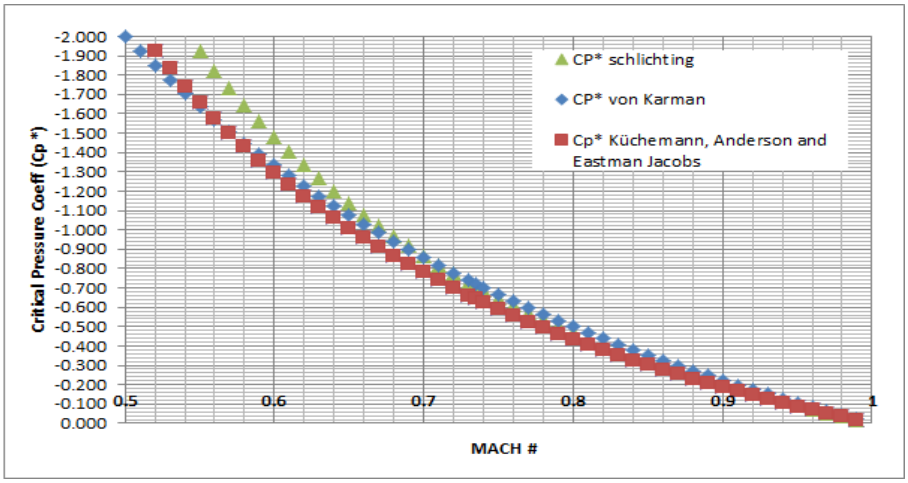

Figure 8. Comparison of *Cp** equations (Schlichting, Von Kármán, Küchemann, E. Jacobs and Anderson) as a function of Mach number.

Although these equations approach zero as the Mach number approaches 1, they differ significantly at lower Mach numbers. Because real aircraft wings must develop lift to sustain flight, incipient shock formation typically occurs in the Mach 0.6 to 0.7 range (for swept wings, this is in terms of Mach number normal to the leading edge). Figure 9 shows the variation of the Critical Mach number implied by the different formulas that occur in this range. A given pressure coefficient can imply a variation of Critical Mach Number as much as *M*~ 0.03 in this region. It is enough of discrepancy to cause performance figures to not be met; if a wing section ostensibly designed for $M_{cr} = 0.66$ actually has a $M_{cr} = 0.63$, the speed corresponding to the onset of drag divergence will likely diminish proportionately.

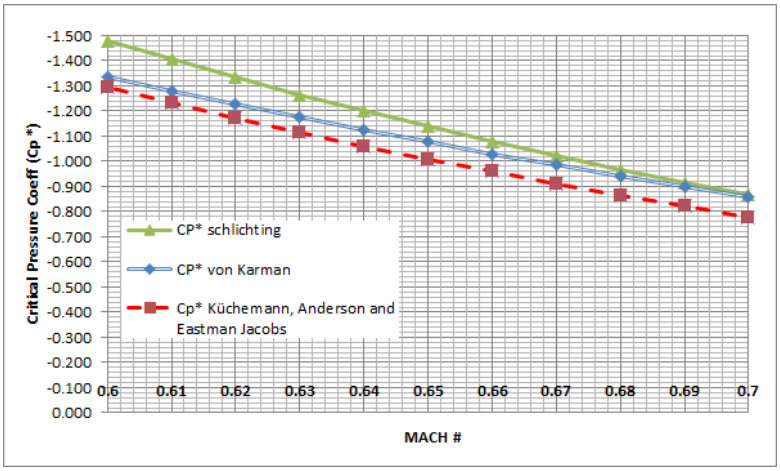

Figure 9. Detailed comparison of *Cp** equations (Schlichting, von Kármán, Küchemann, E. Jacobs and Anderson) as a function of Mach at a typical airfoil design point.

To determine the correct Critical Pressure Coefficient, this thesis turns to computation to compare the equations of Schlichting[8], Von Kármán[7], Küchemann[1], Eastman Jacobs[7], and Anderson[16]. Since the equations of Küchemann, E. Jacobs, and Anderson are all mathematically equivalent for zero sweep, there is no differentiation in the two-dimensional equation. The final differentiation between these equations will be determined with the sweep corrections.

Sweep Corrections

The effects of swept wings on aircraft have been studied since its introduction by Adolf Busemann at the 1935 Volta Congress[2]. Although it has been 81 years since conception, the predictors for shock formation on a swept wing remain inconsistent between authors. Many authors show the original data from the tests inspired by Busemann and explain briefly how sweep delays the onset of compressibility effects on the wing, but refrain from calculating the actual Critical Mach Number, and therefore the Critical Pressure Coefficient for swept and sheared wings.

Busemann's early work shows how the swept wing delays the onset of drag rise. He argues that the sweep decreases the Mach number of the flow normal to the leading edge of the

wing, therefore the Mach dependent compressibility effects follow the leading edge Mach number.

Busemann[2] postulated that a swept wing, of angle φ, acts like an infinite span wing yawed at angle φ to the wind. This indicates that the two-dimensional airfoil section is defined normal to the leading edge instead of a “sheared” wing where the airfoil section is defined in the wind axis. Figure 10 shows the swept wing concept from Busemann. In the early works, Busemann provided the theoretical background to sweep theory, which was then carried out in tests performed by Hurbert Ludwieg[21].

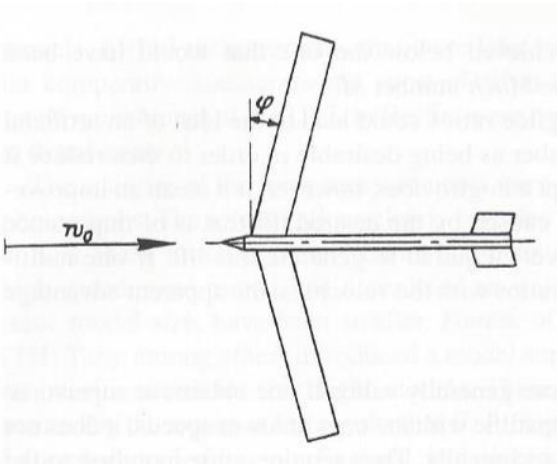

Figure 10. Busemann’s original sketch of the swept wing. Reproduced from Busemann, A. (1935). *Aerodynamischer Auftrieb bei Überschallgeschwindigkeit.*

In 1939, 4 years after Busemann[2] first presented his work on swept wings, Hubert Ludwieg[21] began preparations for tests in the newly operational supersonic wind tunnel in Göttingen. Ludwieg, deputized by Albert Betz, built two models of the same airfoil section, but with different sweep angles. The first was a trapezoidal wing without sweep, and the second a trapezoidal wing with 45 degrees of sweep (see Figure 11). Their work was done on a low-speed airfoil in order to ensure the improvements of sweep postulated by Busemann were easily visable.

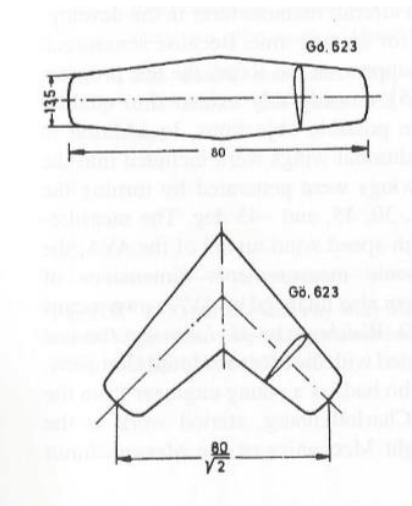

Figure 11. Ludwieg's sketch of the original test wings. Reproduced from Meier, H. (Ed.). (2010). Chapter 1: Historic Review of the Development of High-Speed Aerodynamics (E. Stanewsky, Trans.). In *German Development of the Swept Wing* (pp. 1-68). American Institute of Aeronautics and Astronautics.

The results of Ludwieg's testing can be found in Figure 12. In these results, it can be seen that the swept wing does provide advantage in the higher subsonic regime. This data is taken at $M_\infty = 0.7$ and $M_\infty = 0.9$ with the most notable advantages being seen in the Lift vs. Drag curves. In the straight wing data, there is an obvious increase in drag, that is not present in the swept wing data. This data here confirms Busemann[2] and his work into the advantages of wing sweep.

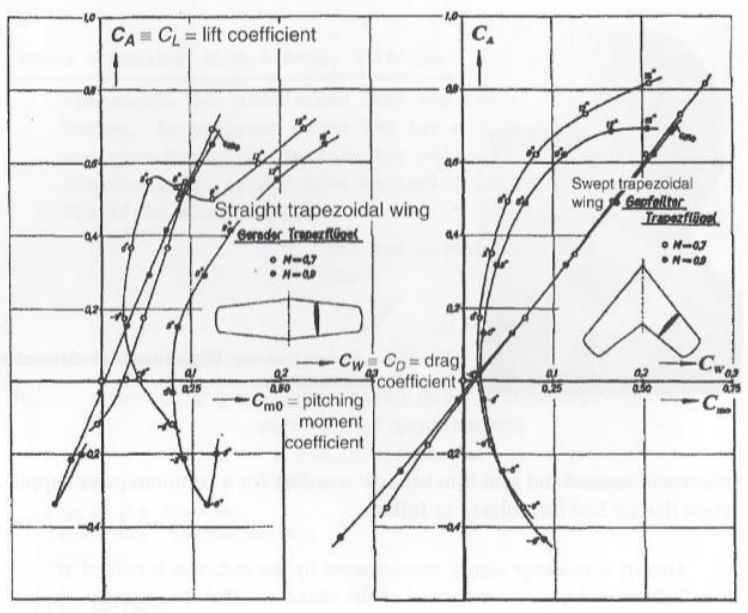

Figure 12. Ludwieg's data from his first swept wing tests. Reproduced from Meier, H. (Ed.). (2010). Chapter 1: Historic Review of the Development of High-Speed Aerodynamics (E. Stanewsky, Trans.). In *German Development of the Swept Wing* (pp. 1-68). American Institute of Aeronautics and Astronautics.

Due to many skeptics to the test program, Ludwieg further expanded these tests[21]. Figure 13 shows the expansion of the test wings for the second round of testing[21]. This time testing included various sweep angles, and a wing with forward sweep. Since Busemann's theory postulated that the Mach number normal to the leading edge was the driving factor, there is no differentiation between a forward swept wing or a swept back wing, in terms of delaying the drag divergence.

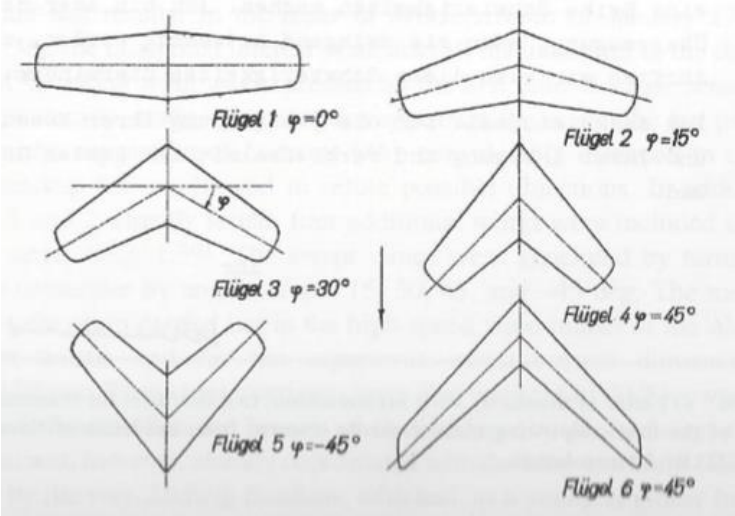

Figure 13. Ludwieg's wings for the expansion of the test program. Reproduced from Meier, H. (Ed.). (2010). Chapter 1: Historic Review of the Development of High-Speed Aerodynamics (E. Stanewsky, Trans.). In *German Development of the Swept Wing* (pp. 1-68). American Institute of Aeronautics and Astronautics.

Once again, Ludwieg found that the effects of sweep postulated by Busemann were correct. The drag coefficient decreases with increasing sweep angle for the flow at $M = 0.8$ as is seen in figure 14. Ludwieg also found that the forward swept wing had almost the same aerodynamic qualities of the swept back wing. These findings prove that Busemann was qualitatively correct in his initial work. However, these tests do not provide the full story.

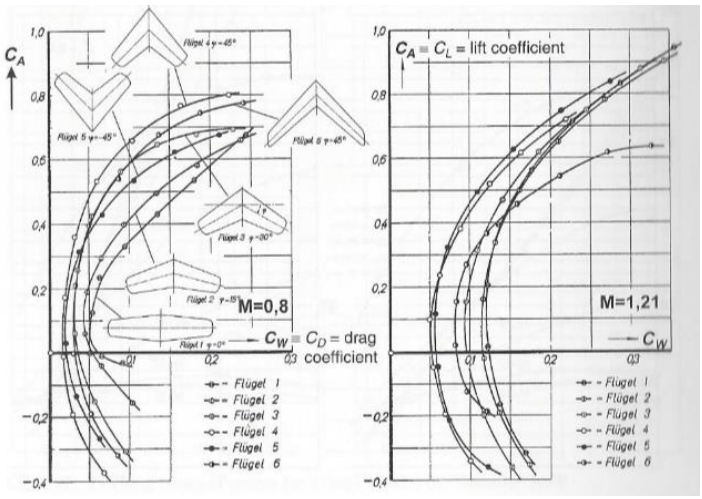

Figure 14. Ludwieg's results from the second round of testing. Reproduced from Meier, H. (Ed.). (2010). Chapter 1: Historic Review of the Development of High-Speed Aerodynamics (E. Stanewsky, Trans.). In *German Development of the Swept Wing* (pp. 1-68). American Institute of Aeronautics and Astronautics.

Jakob Ackeret addressed wing sweep briefly in NACA TM 1320[22]. In this report Ackeret discusses the wind tunnel set up and corrections done in order to test four different sections. The four sections are: 1) unswept 12% thick wing, 2) unswept 9% thick wing, 3) 12% thickness section with 35 degrees sweep, and 4) 9 % thickness section with 35 degrees sweep. Figure 15 shows the results from Ackeret's work.

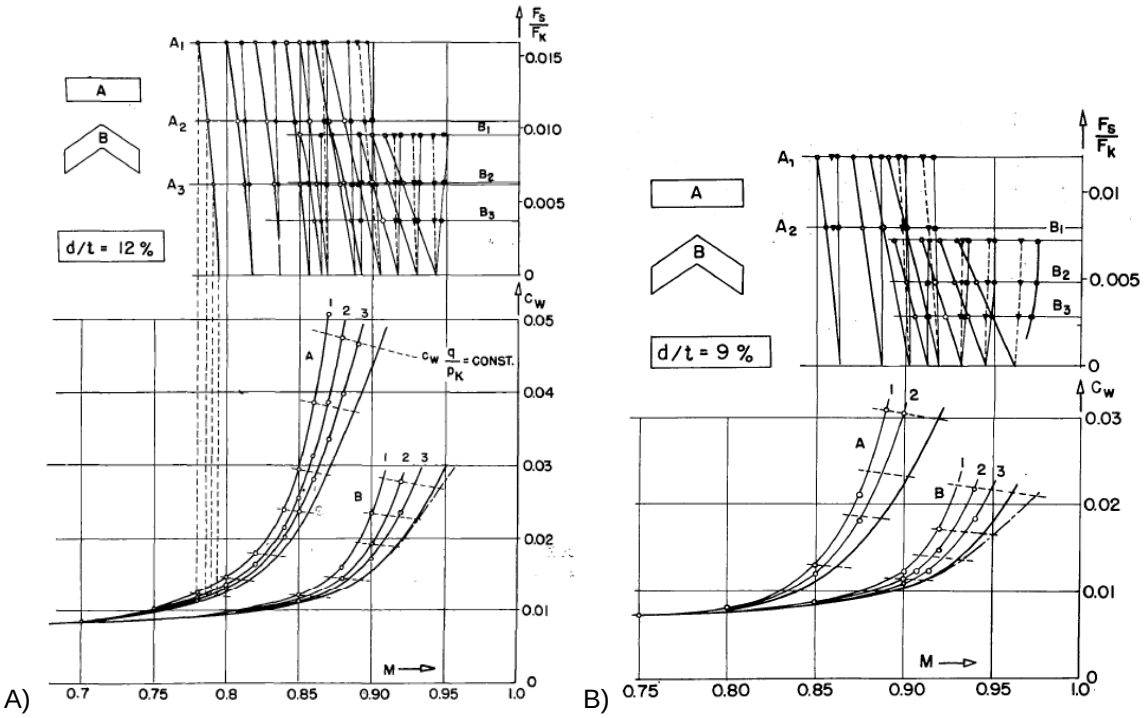

Figure 15. Ackeret test data on A) 12% wing sections and B) 9% wing sections. Reproduced from Ackeret, J., Degen, M. & Rott N. (1951) *Investigations on Wings with and without Sweepback at High Subsonic Speeds*. (National Advisory Committee for Aeronautics TM 1320).

Ackeret[22] does not provide an analytical explanation to the sweep correction. Instead Ackeret provides an experimental fit to the data collected.

Jones[4] cites back to Busemann[2] and Betz[21] (Ludwieg worked for Betz) in his work on High Speed Wing Theory. Jones goes further into the explanation into how the swept wing geometry effects the flow. He argues that the pressure forces on the wing will act normal to its axis and therefore both the pressure drag and the lift should be reduced by $(\cos\varphi)^{2\ 4}$. Jones places a broad transformation here into how the swept wing affects the lift and drag, compared to a straight wing.

The trio of Takahashi, Dulin & Kady[5] employed potential flow solvers to determine the pressure coefficient across swept wings and to correlate the data from Busemann's[2] work to the explanation from R.T. Jones[4]. In their work, Takahashi, Dulin & Kady[5] found that there were some inconsistencies between Jones[4] and Busemann[2]. Instead of the typical cosine squared

transformation, they found that the data fits more to a cosine. However, this work left more questions than answers.

Takahashi & Kamat[6] set to validate Busemann's findings for infinitely swept wings, determine the correction for sheared wings, and further test the findings of Takahashi, Dulin, & Kady[5]. This work employed modern CFD methods to validate the results of the potential flow solvers and determine the correct sweep transformation. For the yawed wing, the authors found that the cosine squared correction matched the data. This indicates that the original description by Busemann[2] was correct. This differs from the results on the sheared wing.

Takahashi & Kamat[6] found that the sheared wing data does not collapse to the explanation given by Busemann[2]. They also find that the cosine correction given by Takahashi, Dulin & Kady[5] does not quite fit the data either. The final works of this paper left more questions unanswered. This thesis set to further investigate the sheared wing sweep comparison based upon this data.

Schlichting[8] approaches the critical pressure coefficient for a sweptback wing of constant chord and infinite span. He argues that the critical condition is dependent upon the flow normal to the leading edge of the wing. This leads to his derivation of the critical pressure coefficient for a swept wing (equation 20a) which is reproduced here.

$$Cp^* = -\frac{2}{\gamma+1}\frac{1-Ma_{\infty_{cr}}^2(\cos\varphi)^2}{Ma_{\infty_{cr}}^2} \tag{20a}$$

The sweep angle enters the numerator of this equation here. The critical conditions are manifested based upon the flow normal to the leading edge and the freestream Mach number.

Küchemann's equation, shown in equation 21a, estimates the critical pressure coefficient for a swept wing.

$$Cp^* = \frac{2}{\gamma M_\infty^2}\left\{\left(\frac{2}{\gamma+1}\right)^{\frac{\gamma}{\gamma-1}}\left(1+\frac{\gamma-1}{2}M_\infty^2\,(\cos\varphi)^2\right)^{\frac{\gamma}{\gamma-1}}-1\right\} \tag{21a}$$

Küchemann derives this equation through the thermodynamic relationships between the static pressure and total head and the local velocity and the sweep of the isobars. In equation 21a the freestream Mach number is found in the numerator and denominator (as seen in the various

equations) yet only applies a sweep transformation to the numerator. The denominator remains dependent upon the freestream Mach number, without the sweep transformation, similar to Schlichting.

Küchemann's[1] sweep transformation is based upon his equation for the local velocity of sound. Shown here in equation 22, Küchemann states that the local sonic velocity is based upon the sweep of the isobars (and therefore the sweep of the wing).

$$\left(\frac{V}{V_0}\right)^* = \{1 + \frac{2}{(\gamma+1)M_\infty^2}(1 - M_\infty^2\,(\cos\varphi)^2\}^{\frac{1}{2}} \tag{22}$$

This equation shows that the sonic conditions of the flow are dependent upon the freestream flow Mach number and the sweep angle of the wing.

In 1949, Stefan Neumark published work on Critical Mach predictions for swept wings[18]. He derived the Critical Mach number for straight untampered wings and then adds his correction of $\cos\varphi$ to each Mach number in the equation, therefore indicating the Critical condition is only dependent upon the Mach number normal to the leading edge.

This differs from Küchemann's and Schlichting's derivation, where the critical condition is defined not only by the Mach number normal to the leading edge, but also the freestream Mach number. This research refers to Neumark's proposed modification in determining the Critical Mach Number, and therefore the Critical Pressure Coefficient, as the "Neumark Modification".

The "Neumark Modification" implies that the sweep corrections should be applied to each Mach number term to the pressure coefficient equation. Equation 23 shows the implied transformation.

$$Cp(M) = Cp(M * \cos\varphi) \tag{23}$$

This differs from Küchemann and Schlichting's derivations of the critical Pressure coefficient. Both authors derived the Pressure Coefficient for a swept wing aircraft, and they both agree that the transformation only occurs to the Mach number in the numerator. This is a major difference that creates the variation in the Critical Pressure Coefficient for a swept wing.

Anderson's[9] equation for the Critical Pressure Coefficient (reproduced in this work as equation 19) does not have a sweep correction.

$$Cp^* = -\frac{2}{\gamma M_\infty^2}\left\{\left[\frac{2+(\gamma-1)M_\infty^2}{\gamma+1}\right]^{\gamma/(\gamma-1)} - 1\right\} \quad (19)$$

This equation is derived based upon thermodynamic relationships, but does not consider its applicability to swept wings. In this work, this equation was modified with the "Neumark Modification" in order to properly transform it into the correct axis frame.

Equation 24 shows Anderson's equation with the "Neumark Modification" for swept wings.

$$Cp^* = -\frac{2}{\gamma M_\infty^2(\cos\varphi)^2}\left\{\left[\frac{2+(\gamma-1)M_\infty^2(\cos\varphi)^2}{\gamma+1}\right]^{\gamma/(\gamma-1)} - 1\right\} \quad (24)$$

In this equation the sweep correction is applied to the numerator and denominator, per Neumark. With this sweep correction, the equation is equivalent to the Eastman Jacobs derivation[7] with the "Neumark Modification".

The derivation from Eastman Jacobs is shown in equation 18, with the sweep correction shown in equation 25.

$$Cp^* = \frac{2\left[1-\left(\frac{2+(\gamma-1)M_\infty^2(\cos\varphi)^2}{\gamma+1}\right)^{\gamma/(\gamma-1)}\right]}{\gamma M_\infty^2(\cos\varphi)^2} \quad (25)$$

This equation has the sweep correction in the numerator and the denominator. Unlike the equations for no sweep, this equation differs from Küchemann. However, this equation is still mathematically equivalent to Anderson's equation with the Neumark Modification.

Von Kármán does not address sweep in his derivation of the critical pressure coefficient in his work dating from 1941[7]. Although it was following the Volta Congress, it predates R.T Jones' work in the United States.

In order to apply Von Kármán's equation to sweep the "Neumark Modification" was used in this research (equation 26).

$$Cp^* = \frac{2\left[\left(1-M_\infty^2(\cos\varphi)^2\right)^{3/2}\cdot\left(1+M_\infty^2(\cos\varphi)^2\right)^{1/2}\right]}{M_\infty\cos\varphi} \quad (26)$$

Once again the sweep correction applies to each Mach number term, in the numerator and the denominator.

Bertin & Cummings[17] addressed swept wings all too briefly in their book Aerodynamics for Engineers. The pair reproduced the data from the original swept wing testing and only discussed the effects of sweep. There is no discussion in designing an aircraft for specified sweep or on the predictors to shock formation on the swept wing.

McLean address wing sweep in his book Understanding Aerodynamics[11]. In his discussion of the swept wing, McLean states that the critical conditions are dependent upon the Mach number perpendicular to the isobars of the wing. Although the isobars should more or less follow the sweep of the wing, this is not always the case and is a distinction from the sweep corrections of various authors.

McLean[11] states that the pressure coefficient of the three-dimensional wing is the two-dimensional data transformed by $(\cos\varphi)^2$.

$$Cp_{3D} = Cp_{2D}(\cos\varphi)^2 \tag{27}$$

This equation by McLean argues that the transformation to the pressure coefficient is the $(\cos\varphi)^2$ but doesn't explain how it is applied. Neumark applies his transformation to the flow normal to the leading edge of the swept wing. McLean suggests that the transformation to the pressure coefficient is a broad application.

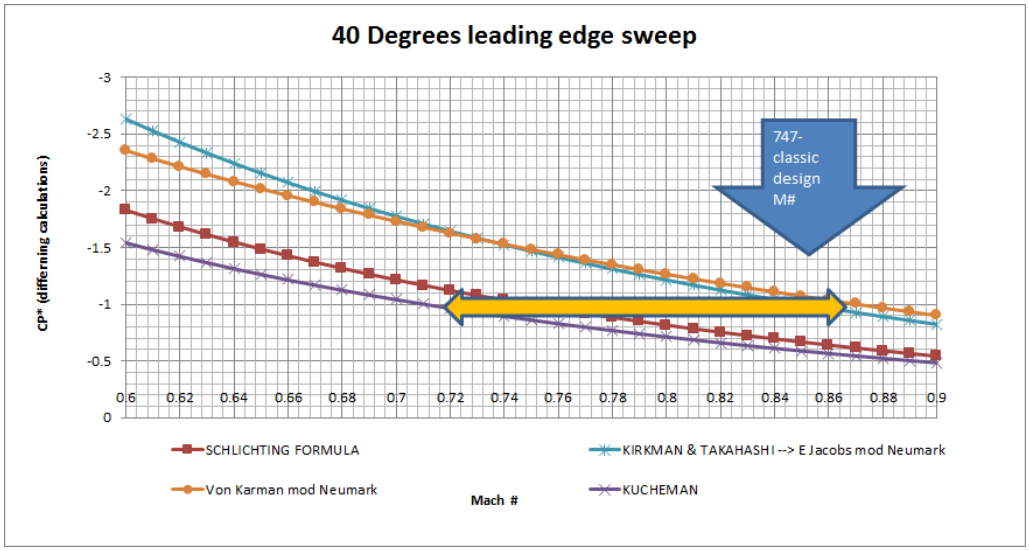

Figure 16. Critical Pressure Coefficient equations for 40 degrees of sweep.

To understand the practical differences between the various Critical Pressure Coefficient equations, each equation was plotted as a function of Mach number and for 40 degrees of sweep. As can be seen in Figure 16, each equation differs significantly between one another. Between these equations, a wing with 40 degrees of sweep, and a minimum pressure coefficient of -1, has a Critical Mach Number range of ~0.72 to ~ 0.84. This is a large discrepancy that could mean the difference in making or missing cruise and performance guarantees for an aircraft. It is this discrepancy that this work set to sort out.

To further understand how the sweep theory applies to gas dynamics, this work turned to the theory of oblique shocks. Although there are some consistencies across authors, many authors do not agree in the explanation in the formation of the oblique shock.

In NACA 1135 the formation of the oblique shock is described as a normal shock to the component of flow perpendicular to the shock wave (Figure 17)[23]. This description lends itself to the sweep principles of Busemann and Jones, where the flow normal to the leading edge (or in this case the shock wave) is important. An interesting point made in NACA 1135 is that the strength of the shock wave is determined from the flow perpendicular to the oblique shock, yet the tangential flow still influences the speed of sound. This important relationship is where further derivations of the oblique shock relationships are found.

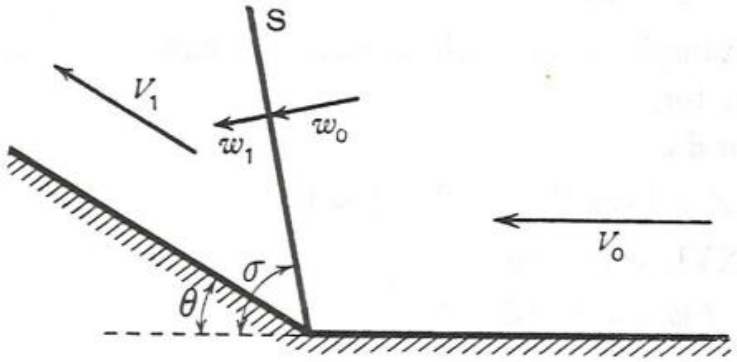

Figure 17. Oblique shock diagram. Reproduced from Milne-Thomson, L. M. (1973). 16.4 Shock Waves. In *Theoretical Aerodynamics* (pp. 302-304). NY: Dover Publications.

COMPUTATIONAL METHODS

In this thesis, necessary computations are performed through legacy open-source aerodynamic codes as well as using commercial computational fluid dynamics (CFD). These computations included running various wings and airfoils at various Mach numbers and angles of attack. The purpose was to gather data to clarify the mysterious phenomena of “stretching” and to determine the “most correct” equation for the Critical Pressure Coefficient of both and unswept, and swept section.

VORLAX

VORLAX is a compressibility-corrected subsonic/supersonic potential flow solver developed by Lockheed-California (now Lockheed Martin) under contract from NASA[14]. The code allows the user to input geometry in three forms: 1) simple, thin flat panels, 2) thin, cambered panels, or 3) a thickness simulating “sandwich panels.” [14] VORLAX outputs a variety of flow solution data: 1) overall force and moment coefficients suitable to build an aerodynamic database (lift, drag, side force, pitching moment, rolling moment, and yawing moment), 2) surface panel net differential pressure coefficients (for thin flat and cambered panels), 3) surface panel actual pressure coefficients (for thickness simulated “sandwich panels), and 4) off-body wake survey velocity vectors. VORLAX was used to determine the correct forms of the various transformations proposed by Schlichting. VORLAX is also used alongside CFD to investigate Critical Mach Number predictive capabilities of the various equations. Because VORLAX is incapable of simulating a shock wave, it can only identify regions of incipient sonic flow where the VORLAX solution will diverge significantly from both reality and a CFD solution.

JAVAFOIL

JAVAFOIL is a simple program built upon a potential flow analysis and a boundary layer analysis[15]. JAVAFOIL uses a higher order panel method to solve the potential flow equations and to obtain an inviscid flow velocity on the airfoil in question. It also implements the criteria set forth by Eppler, to solve the boundary layer differential equations.

JAVAFOIL does not directly simulate supersonic flow. It handles mild transonic Mach numbers through the scaling of the basic potential flow solution through the Kármán-Tsien correction[15]. Although JAVAFOIL includes Critical Mach Number predictive capability; the documentation does not identify the specific equation used to infer either *Cp** or *Mcr*.

The JAVAFOIL applet was used to verify some of the CFD results in low speed conditions, as well as to compare the transonic solutions to the potential flow model.

ANSYS Fluent

ANSYS Fluent software solves the Navier-Stokes equations through either a density-based or pressure-based solver[13]. Due to the analysis of airfoils being in the transonic regime, the density-based solver was used.

In the density based solver of ANSYS, the flow properties are calculated simultaneously. This differs from the pressure based solver, where each of the flow properties are solved individually. The other difference between these equations is the derivation of the governing equations. The pressure based solver derives the continuity equation with the velocity field, where as the density based solver is based upon the continuity, momentum, and energy equations. For transonic flow and shock waves, the governing equations to the density based solver are preferred.

The initial CFD runs were performed using a three-dimensional C-grid with the inlet and outlet placed a large distance from the airfoil in order to prevent interference of the boundaries with the solution. To impose a two-dimensional effect on the airfoil a periodic boundary was applied to the left and right walls. Figure 18 shows the initial three dimensional grid used to calculate the pressure across the airfoil.

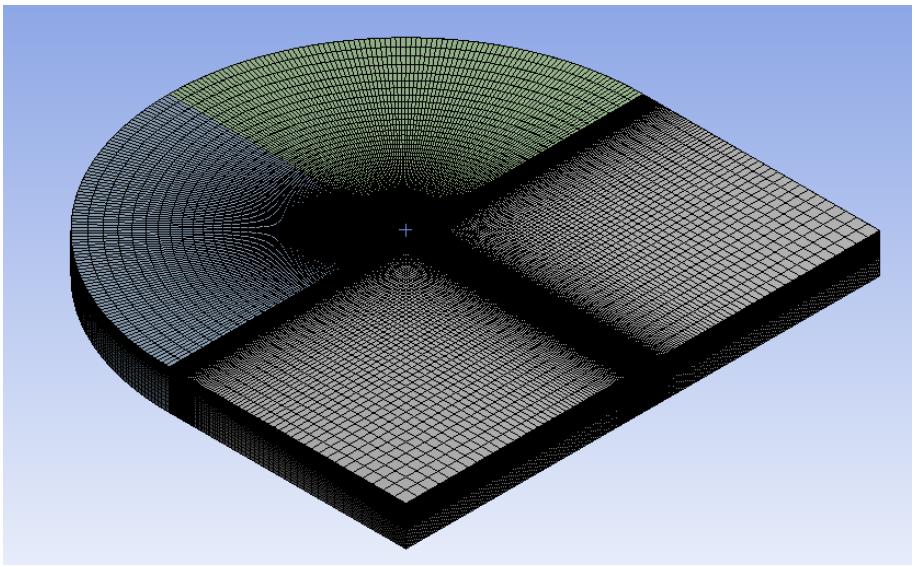

Figure 18. Isometric view of the three-dimensional c-grid.

These runs were done with the steady-state solution option in ANSYS Fluent. This option provides automated solution steering to provide a converged steady solution. The solution steering allows for the code to converge quicker. Ideally this option provides the steady-state solution of the transonic flow properties.

The early runs were set up to verify the Critical Pressure Coefficient equations on an unswept, two-dimensional airfoil section. In these solutions a full three-dimensional grid is unnecessary. Because the grid refinements increased the runtime beyond acceptable limits, the solutions were then switched to run on a 2D grid.

The 2D grid was a C-grid, similar to the 3D grid, with the inlet and outlet boundaries a significant distance from the airfoil itself. Figure 19 shows the two-dimensional grid used for the unswept tests. The grid in this figure shows one of the early grid sizes run in the testing.

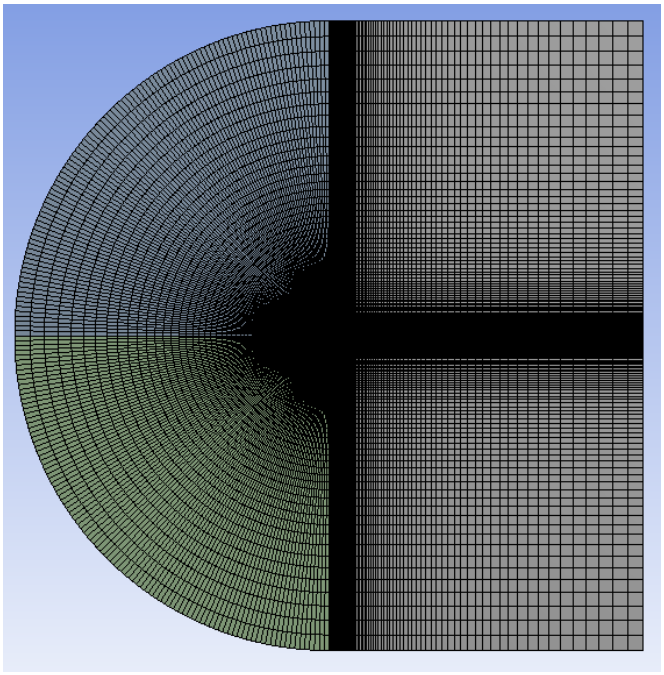

Figure 19. Image of the two-dimensional c-grid used for the unswept airfoil sections.

The 2D runs were also run with the steady-state option. Further grid refinement was done in order to verify the initial solutions. In these grid refinements, the steady-state solution became unstable, providing inconsistent and noisy data. This led to a transient solution to be setup, in search of a stable converged solution.

In calculating the transient solution, a new source of error occurs. In order to calculate an accurate solution, the grid must be refined not only in the step size but also the time step. These solutions were iterated until steady-state, defined where the data over multiple time steps did not vary, was achieved in the flow. The transient setup allowed much finer grids to converge to a stable solution. The final grid around the airfoil is shown in Figure 20. This shows the grid density that was required for the two-dimensional pressure coefficient data to be converged.

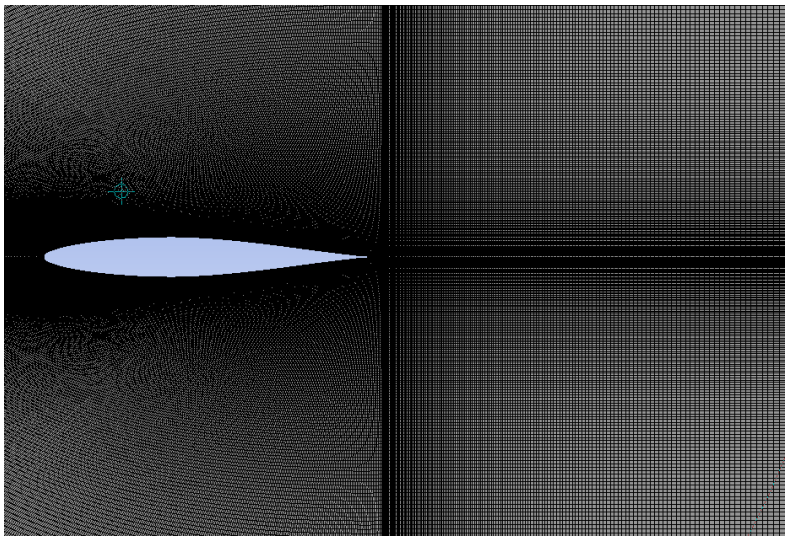

Figure 20. ANSYS Fluent refined grid for the transient solutions.

Once the two-dimensional data provided confident results, the next solutions were done on a three-dimensional C-grid, similar to the first grid run. The goal of these solutions were to apply sweep, however to do so on a quasi 2D airfoil section. The grid was setup normal to the leading edge of a “sheared” wing. This means that the actual airfoil tested is a transformed version of the NACA 64-012[20] airfoil tested.

Figure 21 shows the sweep transformation on the airfoil. In this image the original airfoil is shown as the sketched spline. This airfoil is defined in the wind axis of the wing. The cutout in the figure below shows the airfoil defined off the leading edge of the swept wing. In this figure it can be seen that the thickness form does not change due to sweep, however the airfoil chord is transformed by the cosine of the sweep.

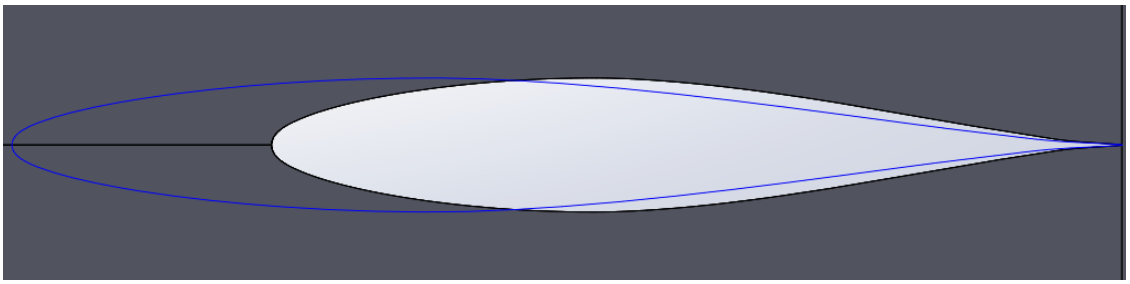

Figure 21. Swept airfoil geometry.

To define the flow velocities in the solution reference frame, the freestream velocities had to be transformed. The coordinate system transformations are shown as equations 28a through 28d. The coordinate system being defined as 1) *x* is the chord wise direction normal to the leading edge, 2) *y* is the spanwise direction, and 3) *z* is the vertical direction, with positive *z* pointing towards the upper surface of the airfoil.

$$V_x = V \cos\varphi \cos\alpha \tag{28a}$$

$$V_y = V \sin\varphi \cos\alpha \tag{28b}$$

$$V_z = V \sin\alpha \tag{28c}$$

Where:

$$V = M * a \tag{28d}$$

These equations are dependent upon an angle of attack, α, and a sweep angle, φ. Due to the geometry effects of the sweep angle on the grid, only the angle of attack and Mach number were varied for each grid setup. For this work, only 40 degrees of sweep was considered, due to the large variance between the Critical Pressure Coefficient equations at this sweep angle.

For each of the solution setups described, the grid refinements followed the same process. The accuracy of the solutions was checked by decreasing the step size, *h*, by a factor of 1.5 from the original grid, and a second time to the modified grid. For the swept sections, computational memory and time were limited, therefore the step size was reduced by a factor of 1.34. This process provided three distinct solutions of the same flight condition, each with a finer grid than the previous. Using a Grid Convergence Index, the accuracy of the coarsest grid can be determined. The process was repeated for each new grid tested, and is not done on each individual flight condition. Since this testing is only done on the actual grid size, it is acceptable to use the same grid across the flight conditions with great confidence.

TRADE STUDIES

This thesis used calculations to run various trades studies to verify the transonic 1relationships described, as well as the correct Critical Pressure Coefficient equations.

The first trades were run to determine the correct transformation of incompressible flow solutions into compressible solutions starting with the Mach number dependent relationships proposed by Schlichting's Aerodynamics of the Airplane[8]. (These were given in this thesis as equations 6 through 16.)

Prandtl-Glauert Effect on Pressure Distribution

The first transformation examined was the transformation on the pressure distribution. According to Schlichting the compressible pressure distribution is related to the incompressible pressure by the inverse of the Prandtl-Glauert parameter: $\frac{1}{\sqrt{1-M_\infty{}^2}}$.

Figure 22 shows the Mach number dependence of pressure coefficients as computed using a VORLAX sandwich panel model. Here, the model is an aspect ratio 20 NACA 0006 section wing. VORLAX is run at three Mach numbers: 0.0, 0.6 and 0.8 and at a variety of angles-of-attack. From the converged solutions, the centerline pressure profiles are extracted. In each case, the pressure coefficients predicted at high speed are compared against an application of equation 11 ($Cp = \frac{1}{\sqrt{1-M_\infty{}^2}} \cdot Cp_{inc}$) to the pressure coefficients predicted at $M_\infty = 0$ (pure incompressible). In Figure 22a, the effects of $M_\infty = 0.8$ flow on the non-lifting wing are shown. The Schlichting approximation matches the VORLAX computation closely, but not exactly. Figure 22b, shows the effects of $M_\infty = 0.6$ oncoming flow to the wing at incidence. Here, the Schlichting approximation matches the VORLAX computation extremely closely, but not exactly.

A) 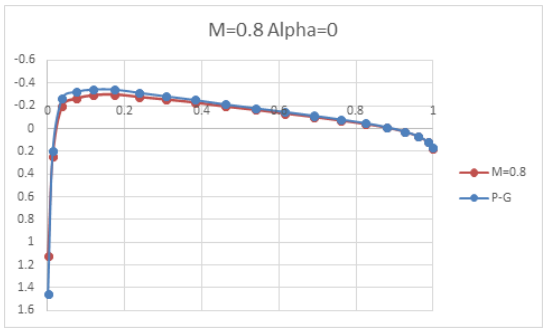

B) 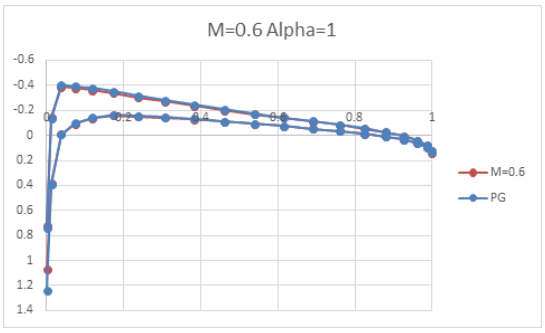

Figure 22. VORLAX sandwich panel solutions. NACA 0006 section. VORLAX run at A) $M_\infty = 0.6$, B) $M_\infty = 0.8$. Prandtl-Glauert predictions based upon VORLAX solutions at $M_\infty = 0.0$.

In the ANSYS Fluent 2-D inviscid compressible flow solution of a NACA 64-012 airfoil section, the results show the Prandtl-Glauert correction to be almost exact for the low transonic flows (around $M_\infty = 0.6$) and a reasonable but imperfect approximation for flow at the higher Mach numbers. Here, the high speed compressible flow solution is compared with an $M_\infty = 0.1$ solution as transformed by equation 11. With the exception of the stagnation point at the leading edge, where Prandtl himself said the correction would be inconsistent[9], the simplified correction provides a good estimation for the compressible solution.

Both VORLAX and ANSYS Fluent agree in many respects. Both solutions find that the induced pressures from thickness follow the Schlichting / Prandtl-Glauert rule; they are all stronger at high speeds than their incompressible equivalents (refer Figure 22a and Figure 23a). For the lifting cases (refer to Figure 22b and Figure 23b), the induced pressures due to incidence, camber and thickness follow the Prandtl-Glauert scaling rule. Thus, both upper and lower high-speed pressure coefficients are noticeably greater than those predicted in incompressible flow; as speed increases the actual wing feels “thicker” than it does at low speeds; it also feels “larger” than it does at low speeds. However, the shape of the incidence dependent pressure profile does not change as expected if there were an effective change in incidence due to “stretching.”

A) 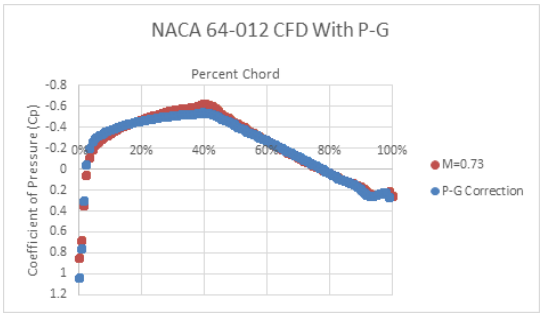

B) 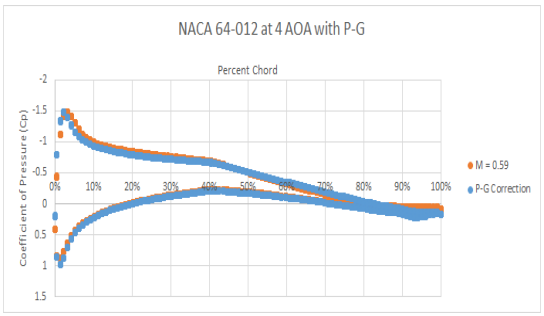

Figure 23. ANSYS FLUENT 2D solutions. NACA 64-012 section. FLUENT run at A) $M_\infty = 0.59$, B) $M_\infty = 0.73$. The Prandtl-Glauert predictions are based upon FLUENT solutions at $M_\infty = 0.1$.

From this evidence, Schlichting's transformation is confirmed from equation 11. At the same time, this evidence refutes "stretching" analogies 1A, 1B and 1D. To explain the noted effects, it is evident that analogy 1C must be true; the "stretching" effect must manifest itself as a non-linear transformation of magnitude of the incoming flow.

Prandtl-Glauert Rule applied to 2D Lift Curve Slope

According to Schlichting's transformations shown in equations 12 and 13, both the lift and the lift curve slope will also contain a Prandtl-Glauert correction. Schlichting argues, since the pressure distribution experiences a transformation in compressible flows, and since the lift is direct integration of the pressures, the lift and lift curve slope will receive the same transformation:

$$\frac{\partial C_L}{\partial \alpha} = \frac{1}{\sqrt{1-M_\infty^2}} \frac{\partial C_L}{\partial \alpha}_{inc}.$$

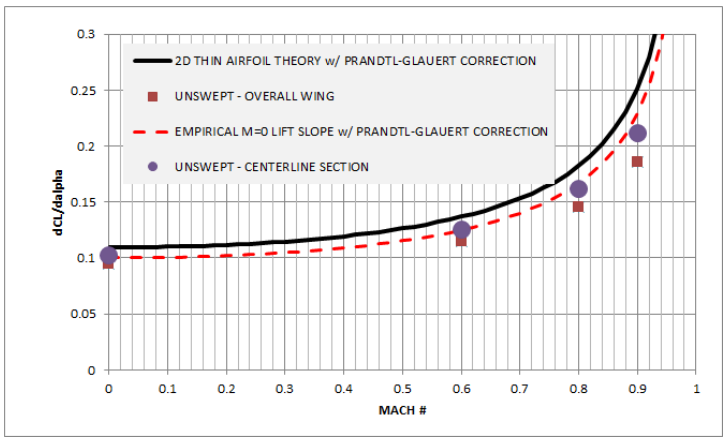

Figure 24. VORLAX solutions on flat plate AR=20 model. The Prandtl-Glauert predictions are based upon VORLAX solutions at $M_\infty = 0.0$.

It can be seen, in Figure 24, how well the lift curve slope of the VORLAX computed compressible solution is approximated by the Prandtl-Glauert correction. One distinction that is found in the VORLAX finite wing data comes from the fact that neither the overall wing lift slope nor the centerline section lift slope of the AR=20 attains the theoretical 2D value. Thus, to make a fair assessment of Schlichting's equations the transformations must "pivot" about the incompressible ($M_\infty = 0$) centerline lift coefficient found in the numerical solution. Following such a procedure, Schlichting' s approximation is nearly exact for the low transonic speeds (around $M_\infty = 0.6$) and slightly differs at higher transonic speeds.

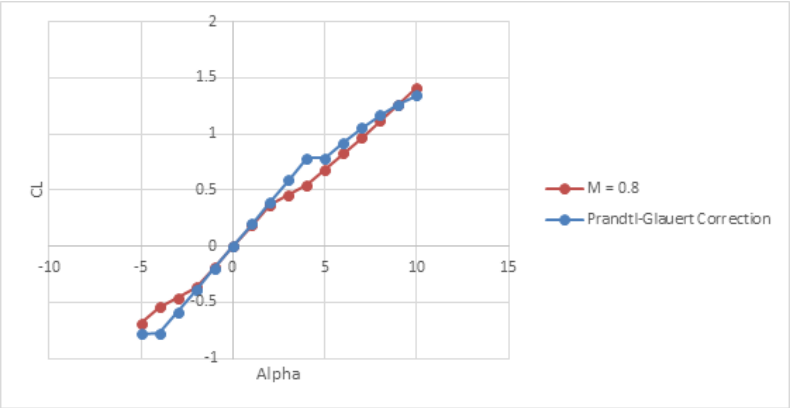

Figure 25. JAVAFOIL solutions of NACA 64-012 2-D model. The Prandtl-Glauert predictions are based upon JAVAFOIL solutions at $M_\infty = 0.0$.

Figure 25 shows the lift curve results from JAVAFOIL for a NACA 64-012 airfoil. Here the code was run at $M_\infty = 0$ and the solution transformed using Schlichting's relationship, comparing it against a solution found running this code at $M_\infty = 0.8$. Because the solution of JAVAFOIL is not a pure inviscid solver, some inconsistencies form between the two solutions due to the Eppler boundary layer model used by this code. However, these results demonstrate that Schlichting's version of the Prandtl-Glauert correction factor on both lift and lift-slope is reasonable.

From this evidence, Schlichting's transformations predicted using equations 12 and 13 are confirmed. At the same time, this evidence refutes the "stretching" analogy 1A. Such a transformation would increase the effective area, but diminish the effective incidence of the wing. There is no such evidence here that analogy 1C is wrong; if the "stretching" effect manifests itself as a non-linear transformation of magnitude of the incoming flow, both the lift and lift-slope of the wing would scale in lockstep with the local pressure coefficients (as Figures 22, 23, 24 and 25 all demonstrate).

Schlichting' s rule for zero lift angle and pitching moment

Schlichting's Transonic Similarity rule includes a correction for the zero-lift angle of the compressible wing; $\alpha_0 = \alpha_{0_{inc}}$. His transformation states that the angle of attack for the compressible wing does not change, and includes that the zero lift angle of the wing should be the same as well.

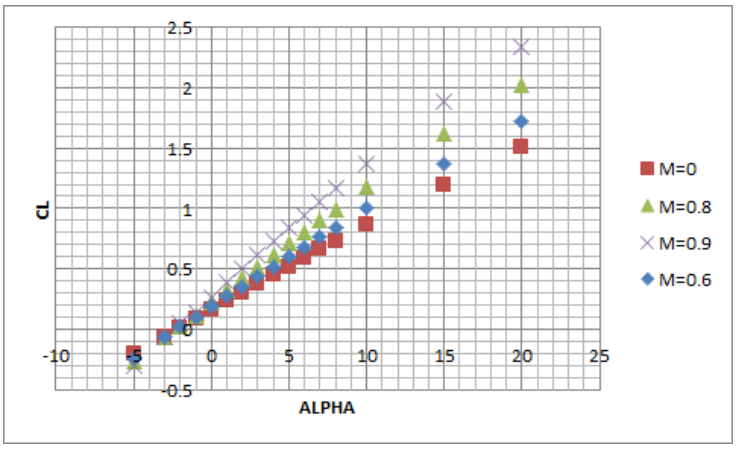

Figure 26. VORLAX solutions of Lift vs. Angle of Attack, on AR=6 thin cambered wing with NACA 23 camber form.

Figure 26 shows the VORLAX solution of a thin cambered wing (NACA 23 camber form) at various Mach numbers and angles of attack with the moment reference point chosen at the wing quarter-chord area centroid. These results, plotting lift as a function of incidence, demonstrate that the zero lift angle of the wing does not vary with Mach number. Schlichting's transformation, or lack of transformation, appears to be correct regarding the zero lift angle.

From this evidence, it is clear that VORLAX continues to substantiate the Figure 1C physical analogy. When the "stretching" effect manifests itself as a non-linear transformation of magnitude of the incoming flow held at a prescribed incidence with respect to the body.

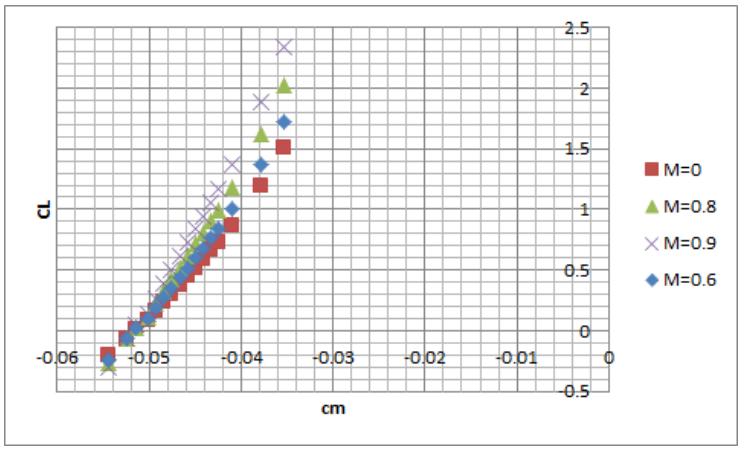

Figure 27. VORLAX solutions of the Pitching Moment vs. Lift on an AR=6 thin cambered wing with NACA 23 camber form.

Schlichting also states that the Transonic Similarity rule should apply the Prandtl-Glauert scaling term to the zero-lift pitching moment as well; that $C_m = \frac{1}{\sqrt{1-M_\infty^2}} C_{m\,inc}$. In Figure 27, the quarter-chord reference pitching moment coefficient against the lift coefficient is plotted. At a first glance the zero-lift pitching moment appears to follow the Prandtl-Glauert correction factor. Under close scrutiny, it becomes clear that the proposed correction is dreadfully wrong. The computational results show a Mach dependent effect that decreases the aerodynamic stability of the wing (moving the aerodynamic center forwards) as the incoming flow increases in speed. In Figures 24 and 26 it can be seen that $\partial C_L/\partial\alpha$ closely follows the Prandtl-Glauert scaling law, the change in the slope of $\partial C_m/\partial C_L$ with Mach number implies that pitching moment cannot follow the same law. In Figure 28, the high speed VORLAX solutions are examined as opposed to incompressible results transformed by $\frac{1}{\sqrt{1-M_\infty{}^2}}$. Here there is a strong disagreement between the direct solution and Schlichting's transformation; Schlichting's method[8] is clearly incorrect.

From this new evidence, there is a situation where VORLAX does not substantiate any proposed physical analogy. If the "stretching" effect manifests itself as a non-linear transformation of magnitude of the incoming flow held at a prescribed incidence with respect to the body, both lift and pitching moment would scale by the same effect and no change in stability would occur.

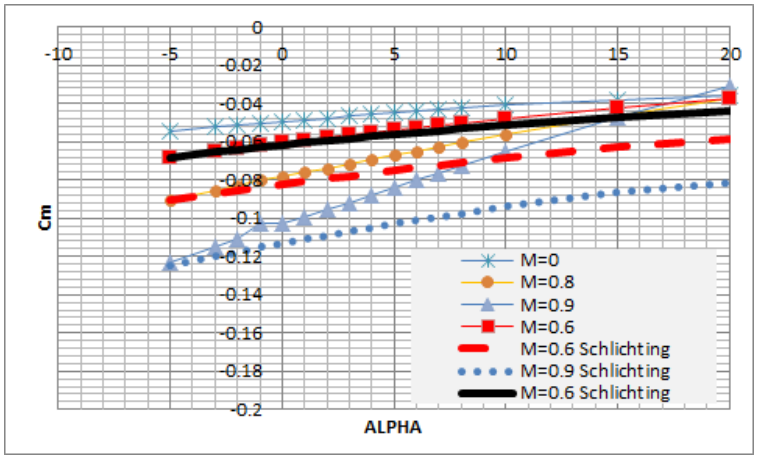

Figure 28. VORLAX solutions of Pitching Moment vs. Angle of Attack on an AR=6 thin cambered wing with NACA 23 camber form.

Schlichting's Rule for Induced Drag

Schlichting's[8] transformation on the induced drag derives from the transformation on the lift as well as his purported spanwise scaling of the wing span; physical analogy 1D. Schlichting also claims that: $C_{Di} = \frac{1}{\sqrt{1-M_\infty^2}} C_{Di_{inc}}$; thus both Lift and Induced Drag scale in lockstep.

Figure 29 plots drag polars of an AR=6 flat-plate wing modelled with 100% analytical credit for leading edge suction. Figure 29A plots, the incompressible solution that builds a drag polar with $\partial C_{Di}/\partial C_L^2 = 0.0555$; pure lifting line theory would predict $\partial C_{Di}/\partial C_L^2 = 0.0530$. Thus, the untwisted wing has a theoretical efficiency of 96%. In Figure 29B, the $M_\infty = 0$ incompressible solution corrected to $M_\infty = 0.9$ using equation 16 is compared against the direct $M_\infty = 0.9$ solution. It can be seen that the correction quickly deviates from the VORLAX solution. Something is dreadfully wrong with Schlichting's rule.

A) 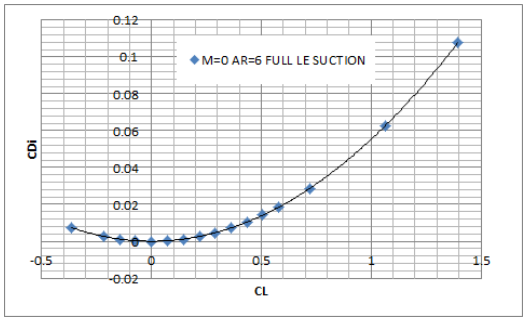

B) 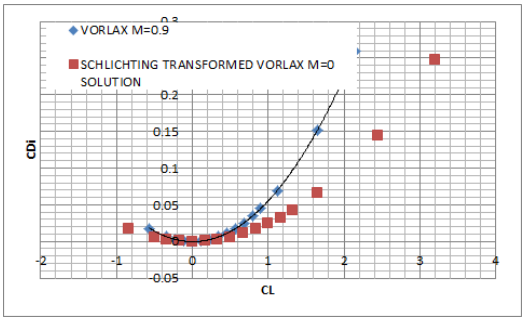

Figure 29. VORLAX solutions on AR=6 thin flat plate wing with 100% credit for leading-edge suction.

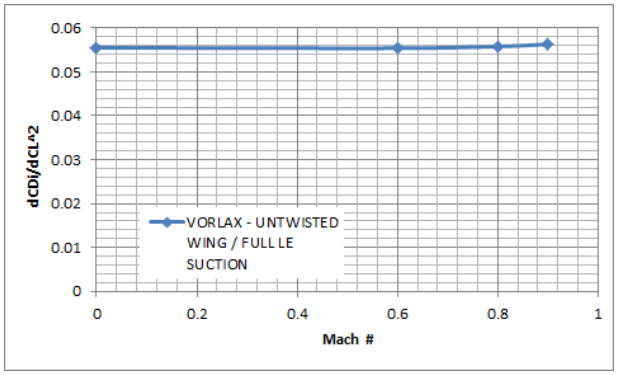

Figure 30. VORLAX solutions on AR=6 thin flat plate wing with 100% credit for leading-edge suction.

Indeed, in Figure 30 $\partial C_{Di}/\partial C_L^2(M)$ is plotted as derived from a series of fully converged VORLAX solutions. Although the slope of $\partial C_L/\partial \alpha$ changes with Mach number, the value $\partial C_{Di}/\partial C_L^2$ remains remarkably constant. In order to match this data, an alternative relationship is proposed as equation 29:

$$C_{Di} = \frac{1}{(1-M_\infty^2)} \cdot C_{Di_{inc}} \tag{29}$$

This is because C_{Di} is predominately a function of C_L^2 if C_L follows a $1/\sqrt{1-M_\infty^2}$ relationship, C_L^2 must follow a $1/(1-M_\infty^2)$ relationship.

From this evidence, VORLAX substantiates the Figure 1C physical analogy. When the "stretching" effect manifests itself as a non-linear transformation of magnitude of the incoming

flow held at a prescribed incidence with respect to the body, lift increases proportionally to the square of enhanced velocity and drag increases proportionally to the square of the lift.

Critical Mach / Critical Pressure Coefficient

As discussed in the Prior Art section of this thesis, many famous authors derived differing equations to estimate the Critical Pressure Coefficient (refer to Figures 8 and 9). Because the equations diverge from one another at lower Mach numbers; where they predict higher critical underpressures (more negative values of *Cp**), this work sets to "experimentally" and "computationally" determine which equations are clearly incorrect and which equations have positive predictive value.

For the transonic 3D wing design problem, designers employ wing sweep to reduce the Mach number normal to the leading edge to approximately $M_\infty \sim 0.6$. It is precisely in this region that the classic equations differentiate themselves from one another. Since real wings carry lift and must contain structure, the designer is particularly interested in the interplay between underpressures created by lift generation (incidence and camber) and those created by thickness. For example, if an initial design relies upon an overly optimistic value of *Cp**, drag divergence will onset early. The aircraft designer will either be forced to live with reduced performance or will need to accept a schedule slip to redesign a thinner (potentially structurally unfavorable) wing.

To begin, wind tunnel pressure test data of a NACA 0012 section was examined[25]. C. D. Harris tested two dimensional flow over a NACA 0012 section at the NASA/LaRC 8-foot transonic pressure tunnel. These tests were performed holding flow velocity constant and changing the Mach number by lowering the static temperature, hence lowering the speed of sound of the flow. The 2D airfoil section was positioned at varying angles of attack to gather upper and lower surface pressure data

High quality published test data confirms the broad utility of all the all the analytical estimation formulas but cannot differentiation between them. Figure 31 examines experimental data collected at $M_\infty = 0.601$ for two different incidences (α=3.86º and α=5.86º). The classic

equations predict *Cp** to be: 1) Schlichting: *Cp**=-1.474, 2) Anderson: *Cp**=-1.288; 3) Jacobs: *Cp**=-1.288; 4) Küchemann: *Cp**=-1.288; 5) Von Kármán, *Cp**= -1.328. Here it is seen that while the equations do differ slightly from one another, the test data cannot differentiate between them. Experiment finds no major shock wave at α=3.86° and a noticeable shock at α=5.86°. Among the analytical predictions, Schlichting's *Cp** equation predicts subcritical flow α=3.86°, while the others predict marginally supercritical flow at that condition. All five equations predict supercritical flow at α=5.86°.

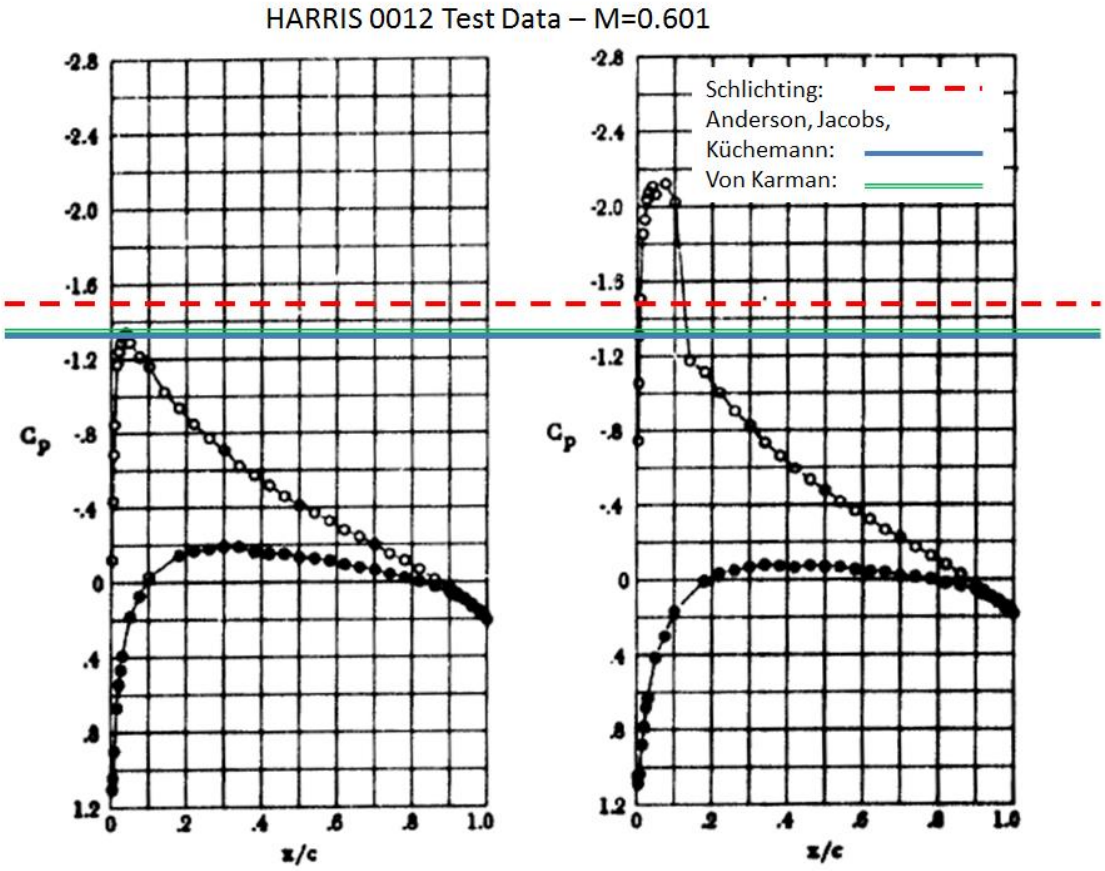

Figure 31. Wind tunnel test data of a NACA 0012 airfoil (2D) at $M_\infty = 0.601$. Adapted from Harris, C. D. (1981). *Two-Dimensional Aerodynamic Characteristics of the NACA 0012 Airfoil in the Langley 8-foot Transonic Pressure Tunnel*. (National Aeronautics and Space Administration TM 81927).

This thesis turns to computation in light of limited available test data, to use this basic procedure to find the best equation suitable to determine the Critical Mach Number, and therefore the Critical Pressure Coefficient.

The calculations in this study used ANSYS Fluent to model a symmetric NACA 64-012 airfoil. Solutions were run varying Mach numbers at two angles of incidence: $\alpha=0^{o}$ and $\alpha=4^{o}$. The calculations began with a low speed solution to estimate the critical condition based upon the equations in the Prior Art section. These solutions were run with a fine sweep of high speed solutions varying the Mach number in 0.01 increments around the predicted critical point to determine the actual conditions associated with the onset of locally supersonic flow.

The process here was slow and methodical. It is crucial to take small increments in Mach number to truly capture the incipient shock formation. Since there is the likelihood of shockless, supercritical flow developing right around the sonic point and there is some difficulty to track the shock wave in the CFD solution, there was careful consideration to document the local Mach number of the near surface flow.

The initial testing on zero degrees angle of attack showed Küchemann[1], Anderson[16] and Eastman Jacobs[7] were correct in the prediction of the shock wave, occurring at $M_{\infty} = 0.74$. However, Schlichting's[8] and Kármán's[8] equations were off by a few hundredths, therefore the next tests set to carry lift on the airfoils in order to force the Critical Mach to occur at lower Mach numbers, where the difference is more noticeable.

A) 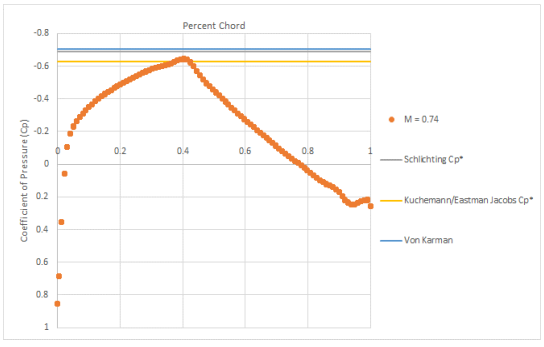

B) 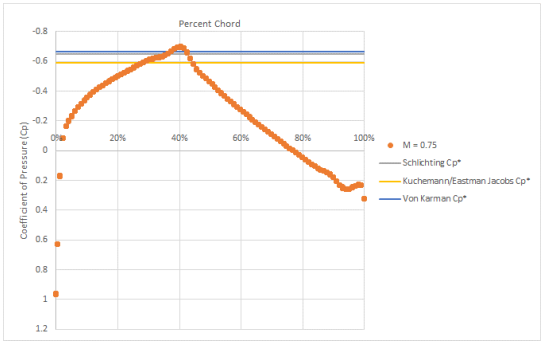

Figure 32. ANSYS Fluent computation on NACA 64-012 airfoil at: A) M∞=0.74; B) M∞=0.75.

Figure 32 plots computed upper and lower surface pressure coefficients of the NACA 64-012 airfoil at zero degrees angle of attack and $M_\infty = 0.74$ and $M_\infty = 0.75$ respectively. At $M_\infty = 0.74$, the shock-wave is in the early stages of forming at the minimum pressure point. Here, the flow just reaches sonic conditions. The Critical Mach Number, is correctly predicted by Eastman Jacobs[7], Anderson[16] and Küchemann[1], but not by Schlichting[8] or Von Kármán[7]. The data here gives compelling evidence that Schlichting[8] and Von Kármán[7] were incorrect in their estimates of the Critical Pressure Coefficient. However, these results conflict with the data obtained at four degrees angle of attack.

In Figure 32b, one can see the strengthening shock-wave on the airfoil. At $M_\infty = 0.75$, each equation predicted the sonic flow on the airfoil section, however this strengthening shock-wave was used to help validate the $M_\infty = 0.74$ results with the weak shock beginning to form.

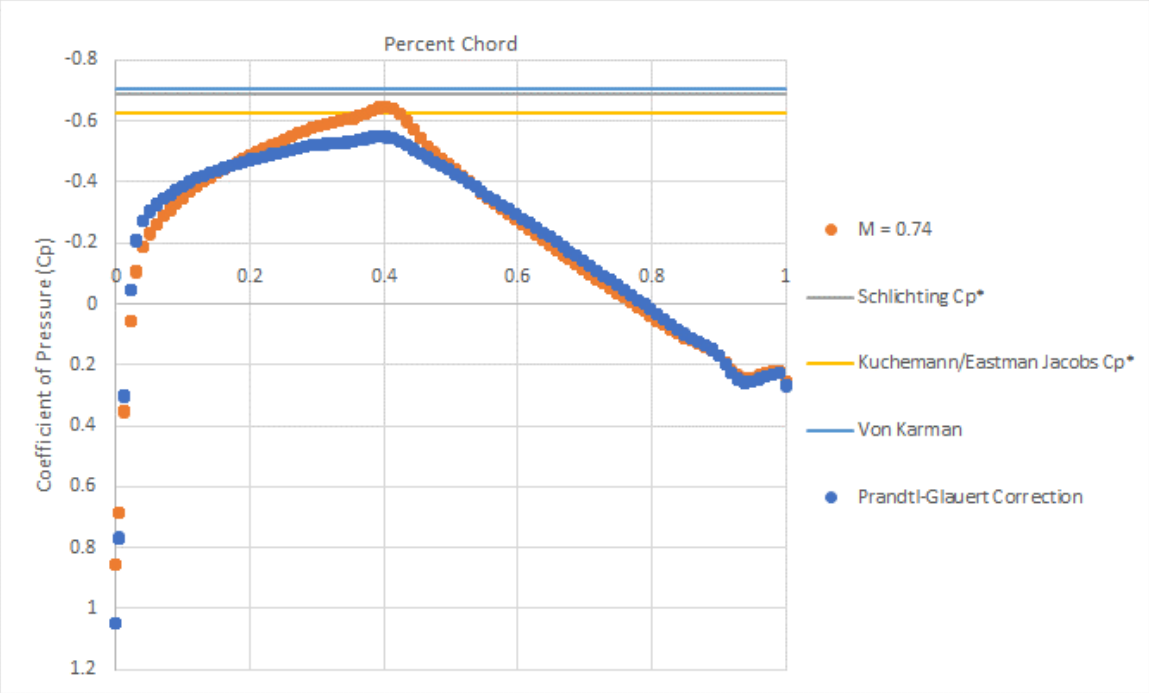

Figure 33. ANSYS Fluent computation on a NACA 64-012 airfoil. Comparison of high-speed vs Prandtl-Glauert corrected low-speed data.

Figure 33 demonstrates the utility and limitations of the simple Prandtl-Glauert transformation[8,9]. This figure compares the low-speed, but Prandtl-Glauert corrected data (using

equation 11) against to the $M_\infty = 0.74$ compressible flow solution from ANSYS. It is possible to see how for high-speed, yet subcritical flow, Prandtl's transformation on the low speed flow is approximate, but reasonably good. There is also evidence of a wider discrepancy around the location of peak underpressure, where local supersonic flow exists; here the approximation is poor.

Table 1

Pressure Coefficient data from ANSYS Fluent compared to the Cirtical Pressure Coefficient based upon the various famous equations.

Mach	NOTES	Cp min	*CP** Schlichting,	*Cp** von Kármán	*Cp** Anderson, Jacobs, Küchemann
0.730	Shock free	-0.6218	-0.730	-0.740	-0.662
0.735	Shock free	-0.6335	-0.709	-0.721	-0.664
0.740	Weak shock	-0.64615	-0.688	-0.703	-0.626
0.750	Weak shock	-0.6980	-0.648	-0.667	-0.591

Table 1 shows the tabulated results of the NACA 64-012 airfoil at zero degrees angle of attack. The data presented above shows the incipient shock-wave beginning to form at $M_\infty = 0.74$. Neither Schlichting[8] nor Von Kármán[7] predict the sonic flow at $M_\infty = 0.74$, based upon the minimum pressure coefficient from the ANSYS solution. The data in this table provides evidence to say Küchemann's and Eastman Jacobs' two-dimensional derivations are correct.

A) 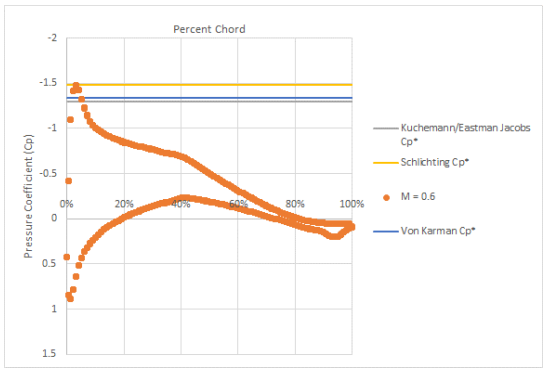

B) 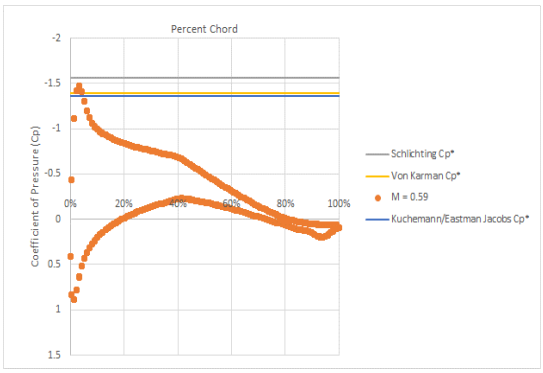

Figure 34. ANSYS Fluent computation on a NACA 64-012 airfoil: A) $M_\infty = 0.590$; B) $M_\infty = 0.600$.

The next testing was done on the NACA 64-012 airfoil at four degrees angle of attack, shown in Figure 34. This solution provided more interesting results. The data showed that at $M_\infty = 0.59$ a shock wave was not forming, and sonic flow was not occurring at the minimum pressure location. This data contradicts the data from the $M_\infty = 0.74$ case. At $M_\infty = 0.59$, only Schlichting's formula does not predict sonic flow. This contradiction does not provide a clear answer to the correct *Cp** equation.

Upon investigation of the solutions, further refinements were done on the solution setup. The first change was to make the solution purely two-dimensional. The grid refinements were done with the steady state solution option, which caused the solutions to become unstable. This led to changing the solution procedure to remove the internal solution steering and calculate a transient solution. With the concerns on accuracy for these solutions, a much finer grid was run with the transient solution.

A grid density study was run to ensure the solutions obtained were converged and accurate. Table 2 shows the grid convergence for the final grid run in the following solutions. The table shows the minimum Coefficient of Pressure, maximum Mach number, with the grid sizing (h) normalized to the finest grid. In the grid refinement checks, the grid is considered acceptable if the asymptotic value approaches 1.

Table 2

Data from the grid refinement on the two-dimensional unswept airfoil sections.

Step Size (h)	**Minimum Pressure (Cp_{min})**	**Maximum Mach**
1	-0.67989	0.9937
1.5	-0.67863	0.9905
2.25	-0.67606	0.9848
Richardson Extrapolation	-0.6811	0.9982
Observed Order (p)	1.766	1.352
GCI_{12} (Error band)	0.221%	0.559%
GCI_{23} (Error band)	0.453%	0.970%
Asymptote	0.99815	0.9967

Figures 35 and 36 shows the results of the transient runs at zero degrees angle of attack at $M_\infty = 0.73$. At this Mach number and angle of attack, the NACA 64-012 airfoil reaches it critical conditions. Figure 35 shows the local Mach number on the airfoil. Although it is not completely evident of a shock wave forming, it can be seen that the local Mach number exceeds 1 on the airfoil. By definition, this is the critical condition on the airfoil.

A)

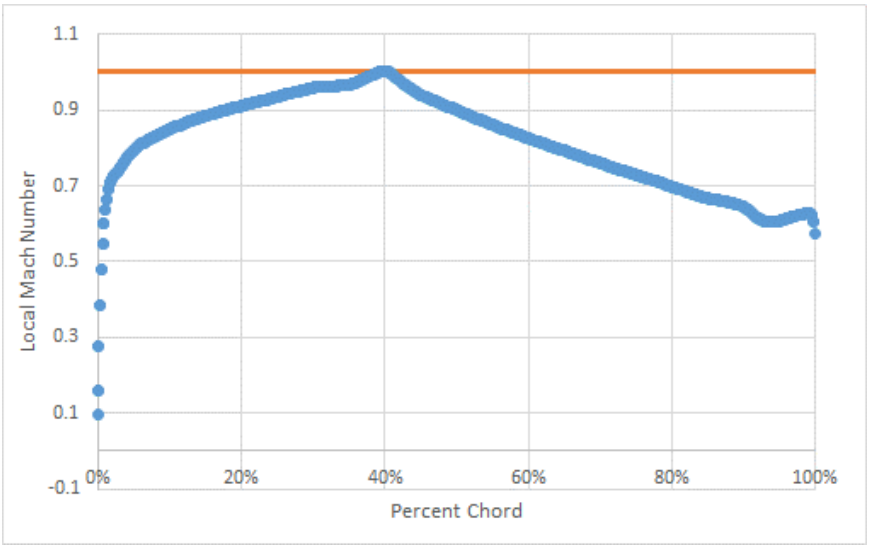

B)

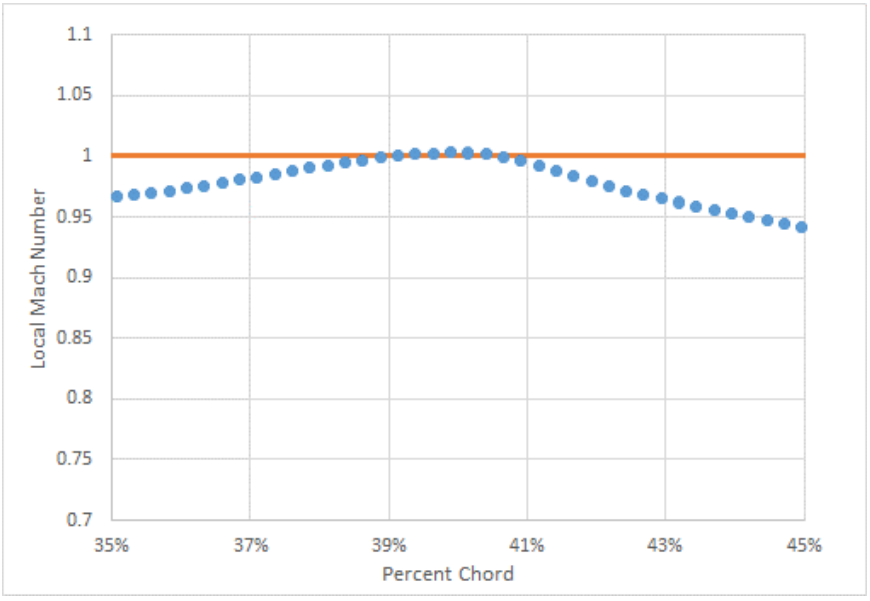

Figure 35. Mach number on NACA 64-012 airfoil section run at $M_\infty = 0.73$ and zero degrees Angle of Attack.

A)

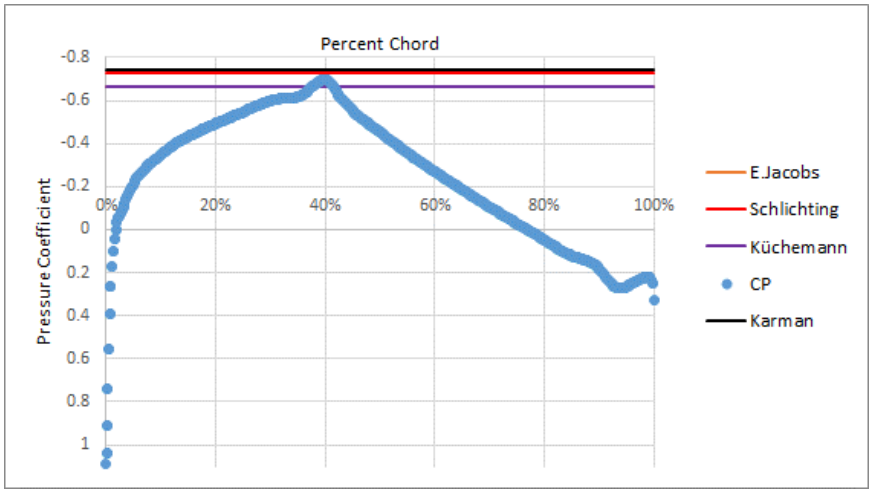

B)

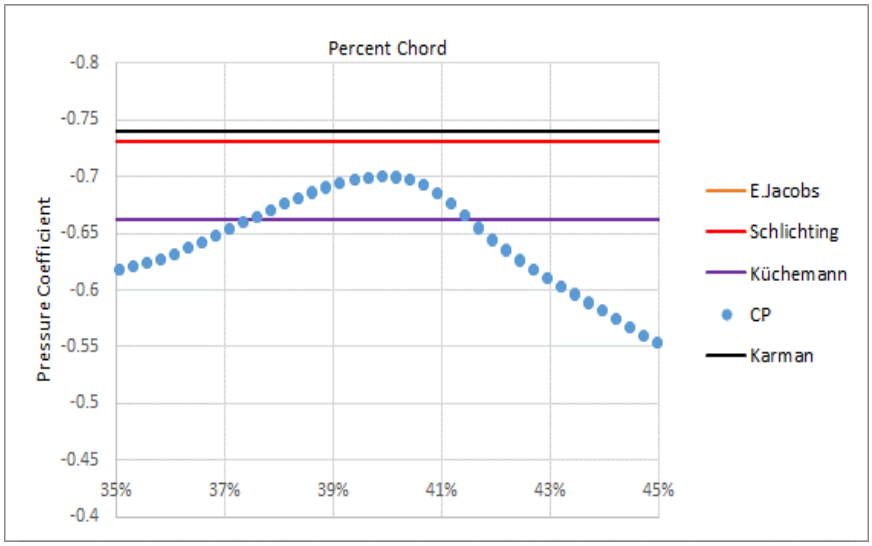

Figure 36. Pressure Coefficient on unswept NACA 64-012 airfoil section run at $M_\infty = 0.73$ and zero degrees Angle of Attack.

Figure 36 shows the Critical Pressure Coefficients from the various equations (Schlichting[8], Eastman Jacobs[7], Küchemann[1], and Kármán[7]) plotted with the pressure coefficient on the airfoil. For the zero degrees angle of attack, the results show that Küchemann's and Eastman Jacobs' formulas are correct in predicting the sonic point on the airfoil. This is similar to the early trades run with the coarse grids.

A)

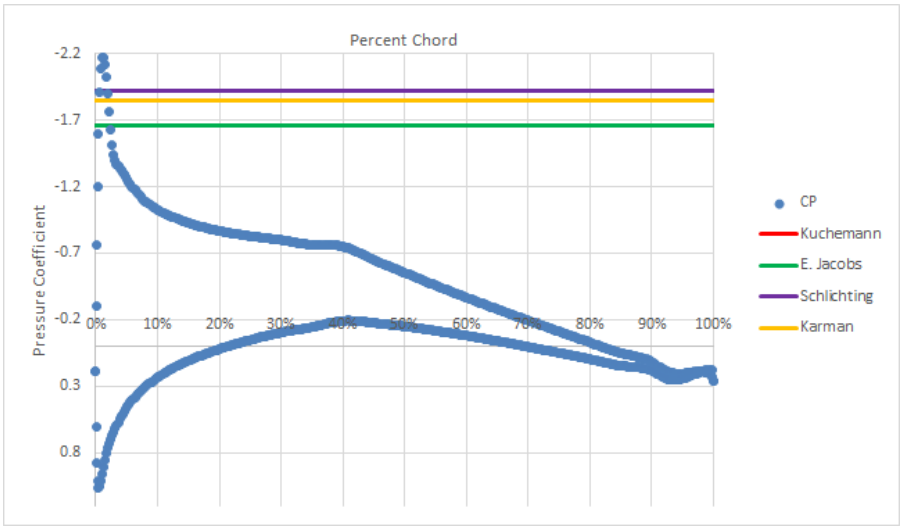

B)

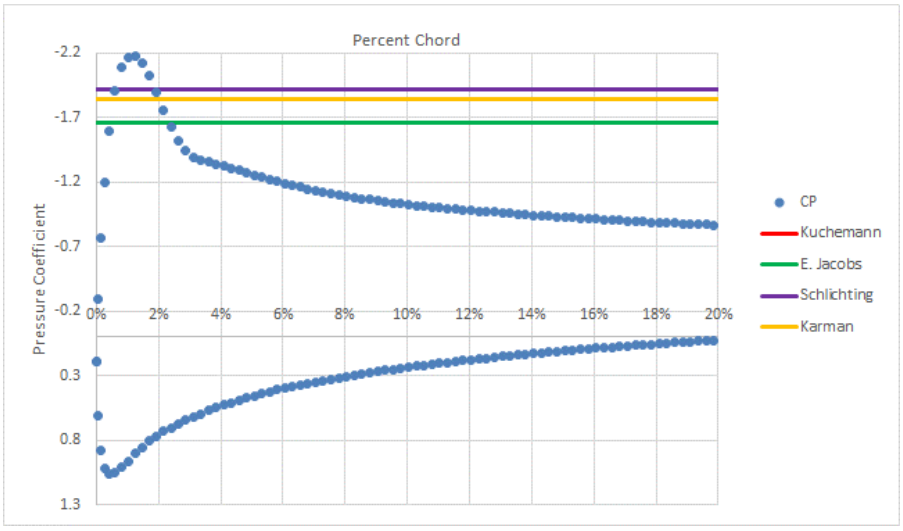

Figure 37. Pressure Coefficient on unswept NACA 64-012 airfoil section run at $M_\infty = 0.55$ and 4 degrees Angle of Attack.

In order to further validate this data, the NACA 64-012 airfoil was run at 4 degrees angle of attack. At $M_\infty = 0.55$ the data clearly shows the strengthening shock wave that forms near the leading edge. Figure 37 shows the results along with the Critical Pressure equations. As can be seen this figure, each equation predicts the critical condition and is considered inconclusive. The next runs set out to determine the Mach number at which the shock wave began to form.

A)

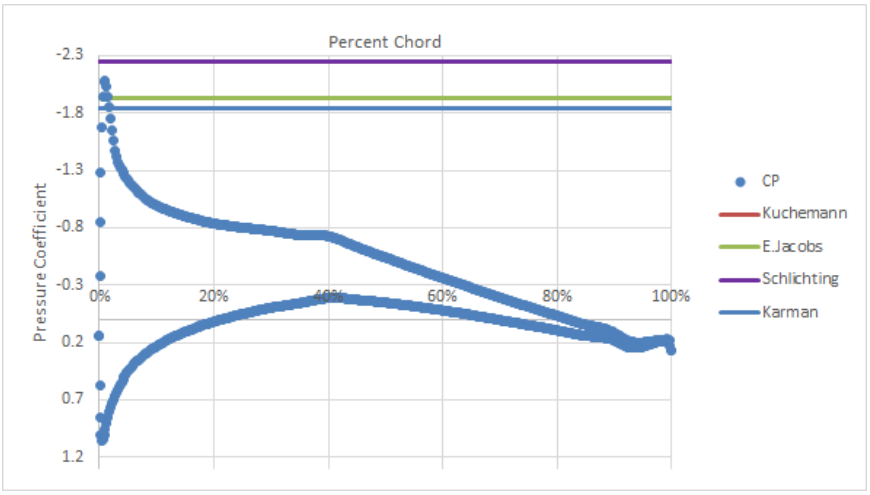

B)

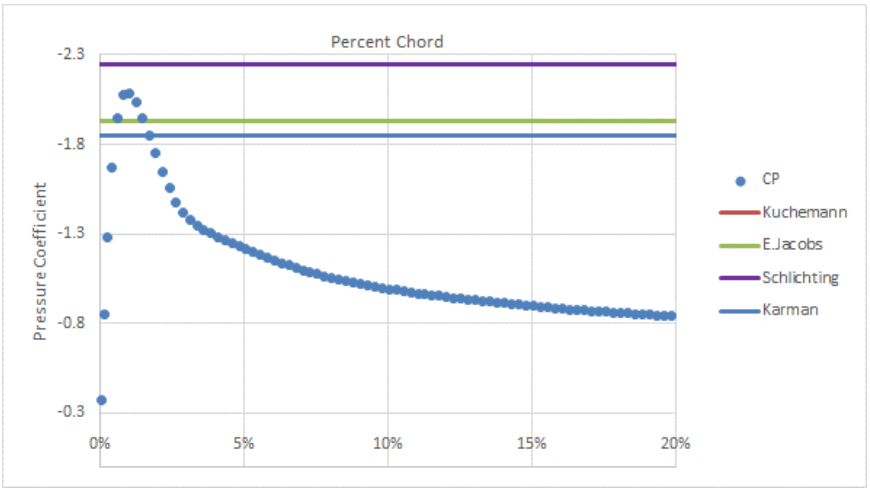

Figure 38. Pressure Coefficient on unswept NACA 64-012 airfoil section run at $M_\infty = 0.52$ and 4 degrees Angle of Attack.

Figure 38 shows the pressure coefficient at $M_\infty = 0.52$ across the airfoil along with the Critical Pressure Coefficient estimations. At this Mach number, the shock wave is just beginning to form, which can be seen near the leading edge of the airfoil. The data here shows that Küchemann[1], Eastman Jacobs[7], and Kármán[7] are correct in predicting this critical location. This leaves that Schlichting is incorrect in his simplified equation.

This two-dimensional flow data proves that Küchemann[1] and Eastman Jacobs[7] are correct in their derivations, for an airfoil without sweep. This is not a complete surprise, as both

Küchemann and Jacobs used thermodynamic flow relationships to reach the final equations for the Critical Pressure Coefficient. The data here from the ANSYS Solutions supports their findings.

Sweep Corrections to the Critical Pressure Coefficient

As discussed in Prior Art section, there are many takes on the necessary correction for estimating the Critical Pressure Coefficient on a swept wing. The final goal of this research is to determine which correction factor accurately predicts the critical conditions across a swept section or, if none of the current methods are found to be correct, determine a correction based upon the sweep of the section.

Figure 16 shows the four Critical Pressure Coefficient equations with 40 degrees applied sweep. The two-dimensional data found that only Eastman Jacobs and Küchemann were correct in accurately predicting the critical conditions. Therefore, only Küchemann[10] and Eastman Jacobs[8], with the Neumark Modification[18], were considered for the corrections. These equations are shown in this paper as equation 21a (Küchemann) and equation 25 (Eastman Jacobs with Neumark Modification) and are reproduced here.

$$Cp^* = \frac{2}{\gamma M_\infty^2}\left\{\left(\frac{2}{\gamma+1}\right)^{\frac{\gamma}{\gamma-1}}\left(1+\frac{\gamma-1}{2}M_\infty^2\,(\cos\varphi)^2\right)^{\frac{\gamma}{\gamma-1}}-1\right\} \tag{21a}$$

$$Cp^* = \frac{2\left[1-\left(\frac{2+(\gamma-1)M_\infty^2(\cos\varphi)^2}{\gamma+1}\right)^{\gamma/(\gamma-1)}\right]}{\gamma M_\infty^2(\cos\varphi)^2} \tag{25}$$

These two equations have very different sweep transformations. Although they are equivalent for an unswept section, they vary vastly with the sweep corrections. In these equations, Küchemann transforms the pressure with the square of the cosine in the numerator only. Eastman Jacobs with the Neumark Modification shows the transformation with the square of the cosine in both the numerator and denominator.

The differences between the equations by Küchemann[1] and Eastman Jacobs[7] is shown in Figure 39 for a sweep angle of 40 degrees. At this sweep angle, the difference is very noticeable, and the same pressure coefficient could mean a critical Mach number around $M_\infty = 0.7$ or $M_\infty = 0.9$ depending upon which equation is correct.

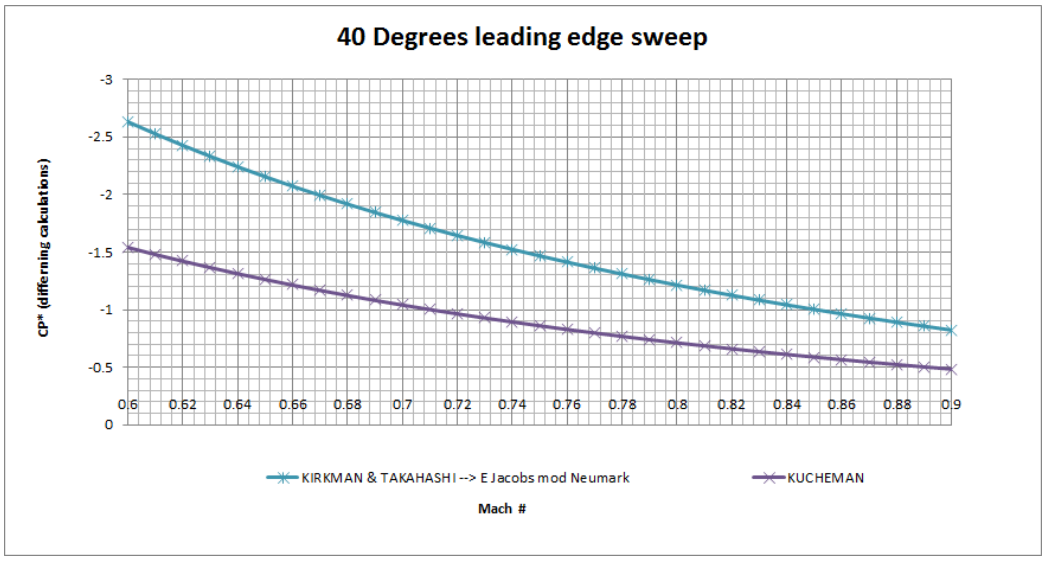

Figure 39. Küchemann and Eastman Jacobs, with the mod Neumark Modification, Cp* equations for 40 degrees of sweep.

The first sweep calculations were done ranging the Mach number from 0.6 to 0.9 by increments of 0.1. Figure 40 displays the results of the early runs. The shock wave begins to form at $M_\infty = 0.8$ and can be seen strengthening in the $M_\infty = 0.9$ solution. This is an early indicator to Küchemann's derivation being correct. In order to verify these solutions, further refinement was done around $M_\infty = 0.7$.

A) 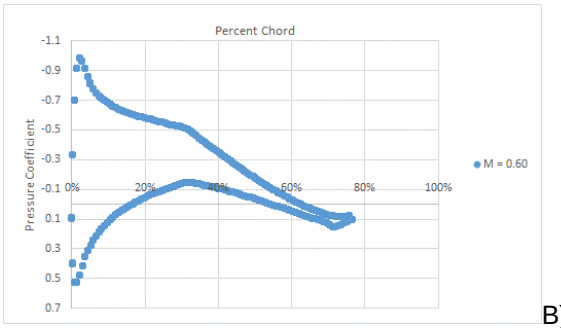

B) 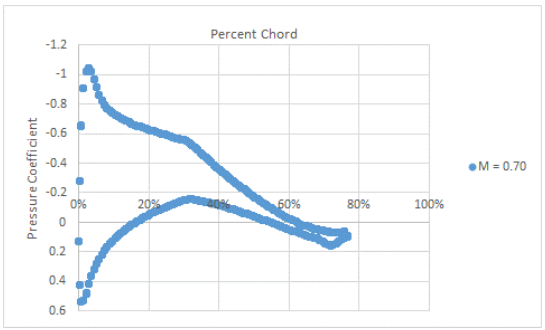

C) 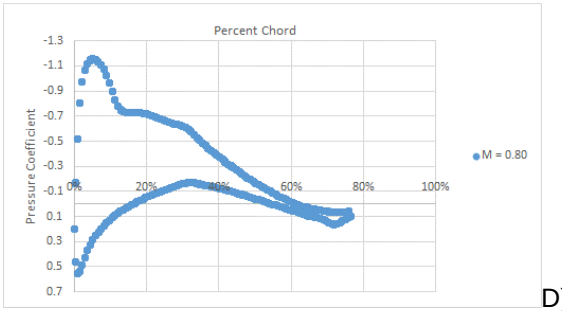

D) 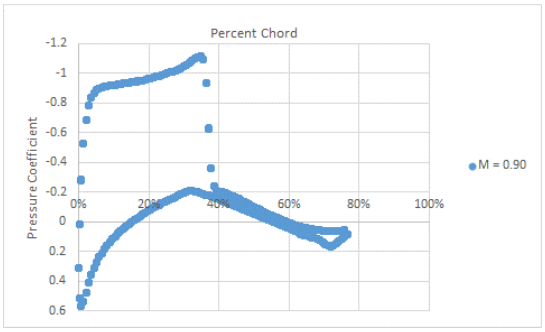

Figure 40. Coefficient of Pressure data from early trades on 40 degree swept airfoil section at 4 degrees angle of attack.

To confirm which equation is correct, the next ANSYS Fluent runs were performed on $M_\infty = 0.72$ with 40 degrees of sweep. At this flight condition, a shock wave is evident. This categorically indicates that Eastman Jacobs with Neumark Modification is incorrect. Figure 41 plots the pressure coefficient from the $M_\infty = 0.72$ run along with the critical pressure coefficient values from Küchemann and Eastman Jacobs with the Neumark modification. In this data it is evident that Küchemann correctly predicts the shock formation.

To further confirm the accuracy of Küchemann[1], the model was reexamined at $M_\infty = 0.7$.

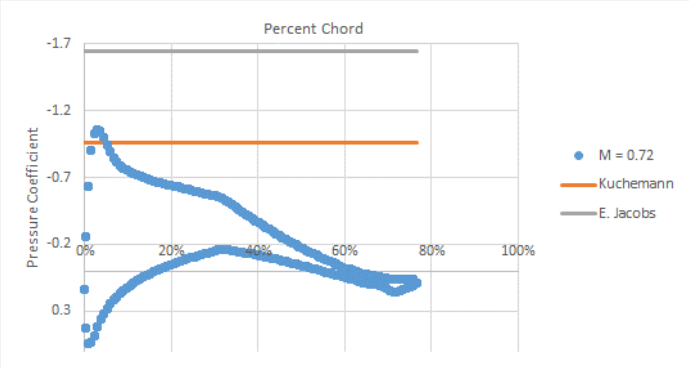

Figure 41. $M_\infty = 0.72$ data on NACA 64-012 airfoil section with 40 degrees sweep run at 4 degrees angle of attack.

Figure 42 shows the data from the $M_\infty = 0.7$ run, where a shock wave is just beginning to form (as is evident from the pressure spike at the leading edge). This figure also plots the critical pressure coefficient value from Küchemann[1] and Eastman Jacobs[7] with the Neumark Modification[18].

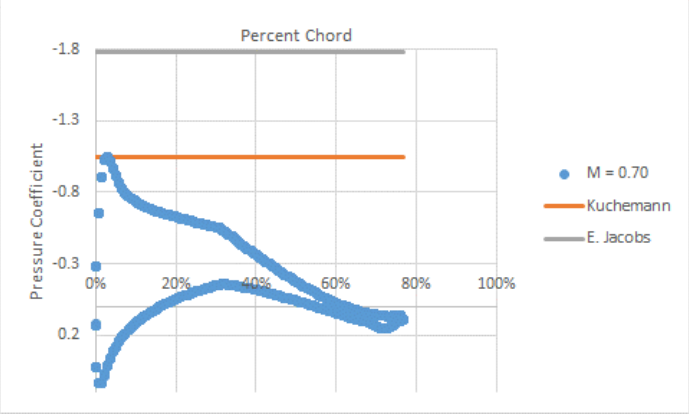

Figure 42. $M_\infty = 0.70$ data on NACA 64-012 airfoil section with 40 degrees sweep run at 4 degrees angle of attack.

In further refinement of this data, a grid convergence was attempted on the $M_\infty = 0.7$ data, however due to limitations on the computational memory, the grid was refined with a step size factor of 1.34, instead of the factor of 1.5 used on the two-dimensional data. There were three grids in total, and the results of the grid refinement are shown in Table 3. The step size, *h*, is normalized to the coarsest grid.

Table 3.

Results of the grid refinement performed on the swept airfoil test sections.

Step Size (h)	**Minimum Pressure (Cp_{min})**	**Maximum Mach**
1	-1.270	1.104
1.34	-1.1569	1.0374
1.80	-1.0434	0.9701
Richardson Extrapolation	-40.05	8.093
Observed Order (p)	0.00995	0.2439
GCI_{12} (Error Bar)	3817%	791%
GCI_{23} (Error Bar)	4203%	850%
Asymptote	0.91092	0.93966

Table 3 shows that the data from ANSYS Fluent does not provide much confidence. This table does show that although the convergence is slow, the data does indeed show convergence. For the purpose of this work, the data from the coarsest grid is used and analyzed. In order to better refine this data, access to improved computing power or methods is required.

Table 3 shows the importance of this research. CFD is a nice tool to work with, however there are many steps that must be taken in order to confirm the resultant data is indeed correct. In the current work, the two dimensional data were able to be completed on a high performance desktop, however the three-dimensional data requires a significant increase in available memory. This means that the same system does not have the ability to build and converge a mesh of the same grid density, due to the three-dimensional aspects. In order to properly converge and verify the three-dimensional data, access to a large computing cluster is required for the necessary memory and computational power.

The data presented here indicates that Küchemann is correct in his derivation of the Critical Pressure Coefficient.

To understand further the physics behind Küchemann's derivation, this thesis revisited his explanations in The Aerodynamic Design of Aircraft.

Küchemann derives the Critical Pressure Coefficient for a swept wing in Chapter 4 of his book. To begin he defines the local sonic condition for a swept wing, reproduced from earlier in this work as equation 22.

$$(\frac{V}{V_0})^* = \{1 + \frac{2}{(\gamma+1)M_\infty^2}(1 - M_\infty^2\,(\cos\varphi)^2\}^{\frac{1}{2}} \tag{22}$$

This equation is derived based upon Küchemann's equation for the local speed of sound. He states this as equation 2.3 in his literature, reproduced here as equation 30.

$$a^2 = a_0^2 - \frac{1}{2}(\gamma - 1)(V_x^2 + V_y^2 + V_z^2 - V_0^2) \tag{30}$$

This is a powerful equation that becomes overlooked often.

Equation 30 from Küchemann, estimates the local speed of sound based upon the perturbation velocities. The total perturbation velocity is shown in the second portion of this equation as: $(V_x^2 + V_y^2 + V_z^2 - V_0^2)$. This shows that the higher the perturbation velocity, the lower the local speed of sound.

Küchemann's derivation is based upon the flow being homenergic (flow in which the sum of the kinetic energy, potential energy, and enthalpy per unit mass is the same at all locations and at all time in the fluid flow)[26] and isentropic, therefore this flow does not account for shock waves. This equation remains valid up until a shock wave occurs in the flow, which will not occur before the local flow exceeds the sonic point.

In order to transform with the proper sweep equation Küchemann derives the equation of motion based upon the transformations found in equations 31a through 31c and 32a through 32c.

$$\xi = x\cos\varphi - y\sin\varphi \tag{31a}$$

$$\eta = x\sin\varphi + y\cos\varphi \tag{31b}$$

$$\zeta = z \tag{31c}$$

$$V_{\xi 0} = V_0\cos\varphi\cos\alpha \tag{32a}$$

$$V_{\eta 0} = V_0 \sin\varphi \cos\alpha \tag{32b}$$

$$V_{\zeta 0} = V_0 \sin\alpha \tag{32c}$$

These transformations can be viewed as figure 43. This figure shows the sketches made by Küchemann and the transformations he makes for the swept wing.

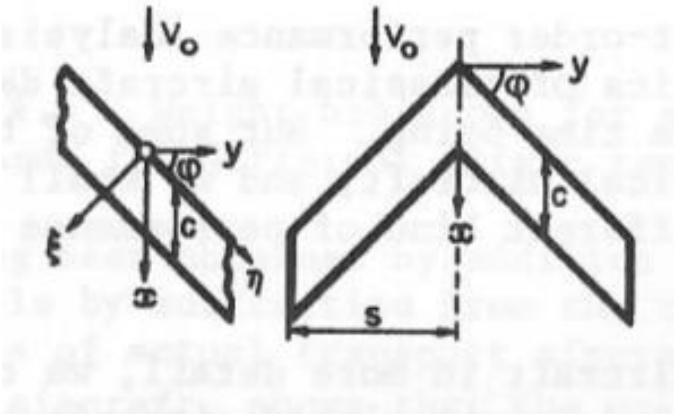

Figure 43. Küchemann's sketch on the coordinate transformation for swept wings. Reproduced from Küchemann, D. (2012). Chapter 4: Properties of Classical and Swept Aircraft. In *The Aerodynamic Design of Aircraft* (AIAA Education Series, pp. 103-221). Reston, VA: American Institute of Aeronautics and Astronautics.

Küchemann does not dispute the claims that the sonic conditions are based upon the flow normal to the leading edge. Instead, he continues to support this claim. Küchemann argues that critical conditions are based upon the flow normal to the leading edge, yet the local speed of sound is still dependent upon the perturbations of the entire flow. It is an interesting claim that Küchemann makes, and one that is similar to the explanation of oblique shock properties from NACA TM- 1135[23].

Küchemann's[1] derivation of the flow around a swept wing is reproduced here as equations 33 through 34b. He states that the flow is governed by:

$$1 - \frac{(\partial\Phi/\partial\xi)^2 + (\partial\Phi/\partial z)^2}{a^2} = 0 \tag{33}$$

Where a^2 is the local speed of sound squared and:

$$\frac{\partial \Phi}{\partial \xi} = V_\xi = V_0 \cos\varphi \cos\alpha + v_\xi \tag{34a}$$

$$\frac{\partial \Phi}{\partial z} = V_z = V_0 \sin\alpha + v_z \tag{34b}$$

In these equations, V_0 is the freestream flow velocity, φ is the sweep angle, α is the angle of attack, and v_ξ and v_z are the perturbation velocities in the ξ and z directions respectively. Therefore, rearranging equation 33 and plugging in 34a for $\partial\Phi/\partial\xi$ and 34b for $\partial\Phi/\partial z$, the equation becomes:

$$V_\xi^2 + V_z^2 = a^2 = V_n^2 \tag{35}$$

Or:

$$V^2 - V_\eta^2 = V_0^2(\sin\varphi)^2\,(\cos\alpha)^2 = a^2 \tag{36}$$

Küchemann indicates the velocity that determines the critical condition is the velocity normal to the leading edge of the wing, whereas the total velocity of the flow could indeed exceed the sonic point. This is shown by equation 36, where the total velocity is shown as, *V*, and the freestream velocity as, V_0.

Küchemann's final derivation of the Critical Pressure Coefficient fundamentally differs from the explanations of Busemann[2] and Jones[4]. In this scenario, Küchemann shows that the Mach number normal to the leading edge does indeed matter, yet this is not the only consideration. With Küchemann's derivations, it is evident he includes the perturbation velocities into his equation and considers a change in the local speed of sound to the flow. This derivation mimics results found in the CFD data gathered.

CONCLUSIONS

This thesis finds that many classical explanations and equations regarding transonic flow around swept wings[2,3,4,7,8,21] are fundamentally inconsistent. The data presented shows that although many of the phenomena described do exist, the various explanations do not fully explain reality.

As a first step in documenting the best formula to estimate the Critical Mach Number of a wing from a potential flow solution, this work revisited the Transonic Similarity Rule. Close

reading of the primary and secondary source literature revealed a multitude of differing interpretations and explanations of the physical transformation implied by the foundational mathematics. The famous authors[2,7,8,11,12,21] all state that there is a geometrical transformation, causing a change in the wing area, aspect ratio, thickness and incidence. Some authors[8,21] hand wave through the explanation to state there is only a difference in the results. These conflicting explanations do not give insight into the actual "stretching" that is applied to the compressible flow. Through the use of VORLAX, CFD (ANSYS Fluent), and some JAVAFOIL solutions, there is evidence to suggest that the geometrical "stretching" explanation does not properly describe the solutions.

Schlichting[8] summarized the Prandtl-Glauert transformations as part of the Transonic Similarity Rule. He provided a table of all of the transformations that should occur, including geometric "stretching". In the work of this paper, Schlichting is found to have the correct transformation for the pressure distribution, the lift curve slope, zero lift angle, and the lift coefficient. These correlations imply that the "stretching" is not geometric, but instead a Mach dependent velocity "scaling" applied to the flow.

Schilichting's transformation of the coefficient of pitching moment and the induced drag does not match the compressible solution. The pitching moment transformation cannot follow the Prandtl-Glauert transformation due to the coupling of the lift transformation, as well as a Mach transformation on the aerodynamic center. The transformation on the induced drag is defined by Schlichting as the transformation on the lift as well as the transformation on the Aspect Ratio. This transformation is defined by a velocity "stretching" in the lift coefficient, and a geometric transformation through the decrease in the Aspect Ratio. The data gathered shows that this transformation is not correct. Instead the drag due to lift scales with the square of the high speed lift coefficient: an effective scaling transformation factor of a $1/(1-M_\infty^2)$ as opposed to Schlichting's $1/\sqrt{1-M_\infty^2}$ relationship.

Evidence shows that most of the manifestations of the Prandtl-Glauert rule that have previously been explained by some sort of "stretching" can be better explained by a velocity "scaling" analogy. Data presented here shows that various proposed transformations of high

speed geometry into an altered, equivalent incompressible solution geometry introduce an effective angle of attack change, area change or aspect ratio change that has been contradicted by the computational results of accepted codes. Therefore, this work refutes the geometrical "stretching" explanation and proposes that the "stretching" is merely a "scaling" of the velocity.

This work found many different published equations that purport to estimate the Critical Mach and Critical Pressure Coefficient, and hence predict the onset of sonic flow. When applied to a transonic aircraft design problem these equations vary significantly from one another.

Using ANSYS Fluent to solve the Navier-Stokes equations, this work set forth to determine which equation is correct in estimating the Critical Pressure Coefficient. The current data shows that for an unswept section, the equations proposed by Küchemann, Eastman Jacobs, and Anderson are all correct. The equations by these three authors are mathematically equivalent for the unswept section and accurately show the sonic conditions forming on the airfoil section.

The next step in determining the correct critical pressure coefficient equation, sweep was applied. In this scenario the various equations were modified either as specified by the author (Küchemann), or modified as postulated by Neumark (Anderson and E. Jacobs). These various sweep corrections provided vastly different results for the Critical Pressure Coefficient.

The ANSYS Fluent solutions for the swept sections do not provide complete confidence in the data gathered. The grid refinement shows that the data does indeed converge, albeit a slow convergence. The issues with the data here result from a lack of memory available for the three-dimensional solutions. Although it is not ideal, the grid refinements were showing the expected trend in the data, which showed the shock wave strengthening with the finer grid resolutions. In order to further verify this data, further grid refinements must be completed on systems with improved computing power. The data must be built and run on a much finer grid and confirmed with the results presented here to ensure true convergence of the CFD data.

The data presented from the swept wing sections show that Küchemann's derivation is indeed correct. Küchemann[1] postulated that the Critical Pressure Coefficient is depended upon the freestream Mach number and the Mach number normal to the leading edge. This is similar to

Schlichting[8] but differs from the work of Neumark[18]. Küchemann does not dispute the claim that the flow normal to the leading edge must exceed the sonic condition, however he does argue that the sonic condition is a function of the total perturbation velocity from the freestream. Therefore, the freestream Mach number still has importance in determining the Critical Pressure Coefficient.

This revelation indicates that Von Kármán's Transonic Similarly Rule (as described by Schlichting[8]) is indeed incorrect in its explanation. Kármán does not consider the effects of a nonlinear scaling on the velocity perturbations and only concerns himself with the possible explanation of a geometric scaling. Therefore, the transformations from an incompressible to compressible flow is not a geometric stretching, but indeed a velocity scaling.

REFERENCES

[1]Küchemann, D. (2012). *The Aerodynamic Design of Aircraft* (AIAA Education Series). Reston, VA: American Institute of Aeronautics and Astronautics.

[2]Busemann, A. (1935). *Aerodynamischer Auftrieb bei Überschallgeschwindigkeit.* Luftfahrtforschung Vol. 12, No. 6, 1935, pp. 210-215.

[3]Jones, Robert T. (1945) *Wing Plan Forms for High-Speed Flight* (National Advisory Committee for Aeronautics TR 863).

[4]Jones, R. T., & Cohen, D. (1960). *High speed wing theory*. Princeton, NJ: Princeton University Press.

[5]Takahashi, T. T., Dulin, D. J., & Kady, C. T. (2014). *A Method to Allocate Camber, Thickness and Incidence on a Swept Wing.* (American Institute of Aeronautics and Astronautics). AIAA 2014-3172.

[6]Takahashi, T. T., & Kamat, S. (2015). *Revisiting Busemann: The Design Implications of Inconsistencies Found Within Simple Sweep Theory*. (American Institute of Aeronautics and Astronautics). AIAA 2015-3376.

[7]Von Kármán, T. (1941). Compressibility Effects in Aerodynamics. *Journal of the Aeronautical Sciences, 8*(9), 337-355.

[8]Schlichting, H., & Truckenbrodt, E. (1979). Aerodynamics of the Airplane (H. J. Ramm, Trans.). McGraw-Hill.

[9]Prandtl, L. (1935) *General Consideration on the flow of Compressible Fluids* (National Advisory Committee for Aeronautics TM 805).

[10]Göthert, B. (1946). *Plane and Three-Dimensional Flow at High Subsonic Speeds*. (National Advisory Committee for aeronautics TM. 1105).

[11]McLean, D. (2013). 7.4.8 Airfoils in Transonic Flow. In *Understanding Aerodynamics* (pp. 342-350). John Wiley & Sons.

[12]Drela, M. (2014). 8.6 Prandtl-Glauert Analysis. In *Flight Vehicle Aerodynamics* (pp. 173-180). MIT Press.

[13]SAS IP, Inc., *Section 20.1.2. Density-Based Solver*, The ANSYS Fluent Getting Started Guide, Release 15.0

[14]Miranda, L. R., Baker, R. D., & Elliott, W. M., (1977) *A Generalized Vortex Lattice Method for Subsonic and Supersonic Flow* NASA CR 2875.

[15]Hepperle, M. (2007, January 27). JavaFoil. Retrieved October 29, 2015, from http://www.mh-aerotools.de/airfoils/javafoil.htm

[16]Anderson, J. (2005). 5.9 Critical Mach Number and Critical Pressure Coefficient. In *Introduction to Flight* (Fifth ed., pp. 283-294). New York, NY: McGraw Hill.

[17]Bertin, J. J., & Cummings, R. M. (2014). 9.4 Swept Wing at Transonic Speeds. In *Aerodynamics for Engineers* (Sixth ed., pp. 527-543). Pearson.

[18]Neumark, S. (1949). *Critical Mach Numbers for Thin Untapered Swept Wings at Zero Incidence*. (Aeronautical Research Council Reports and Memoranda No. 2821).

[19]Glauert, H. (1927). *The Effect of compressibility on the Lift of an Aerofoil*. (Royal Aeronautical Society).

[20]Abbott, I. H. & Von Doenhoff, A. (1949) *Summary of Airfoil Data*. (National Advisory Committee for Aeronautics No. 824)

[21]Meier, H. (Ed.). (2010). Chapter 1: Historic Review of the Development of High-Speed Aerodynamics (E. Stanewsky, Trans.). In *German Development of the Swept Wing* (pp. 1-68). American Institute of Aeronautics and Astronautics.

[22]Ackeret, J., Degen, M. & Rott N. (1951) *Investigations on Wings with and without Sweepback at High Subsonic Speeds*. (National Advisory Committee for Aeronautics TM 1320).

[23]*Equations, Tables, and Charts for Compressible Flow*. (National Advisory Committee for Aeronautics Report 1135).

[24]Milne-Thomson, L. M. (1973). 16.4 Shock Waves. In *Theoretical Aerodynamics* (pp. 302-304). NY: Dover Publications.

[25]Harris, C. D. (1981). *Two-Dimensional Aerodynamic Characteristics of the NACA 0012 Airfoil in the Langley 8-foot Transonic Pressure Tunnel*. (National Aeronautics and Space Administration TM 81927).

[26]Homenergic Flow. (n.d.). Retrieved March 25, 2016, from http://encyclopedia2.thefreedictionary.com/homenergic flow